Diplomarbeit

Evaluation of a magnesium-based implant in the growing rat model

eingereicht von

Lisa Paar

zur Erlangung des akademischen Grades

Doktor(in) der gesamten Heilkunde

(Dr. med. univ.)

an der

Medizinischen Universität Graz

ausgeführt an der

Universitätsklinik für Orthopädie und Traumatologie

unter der Anleitung von

Univ.-Ass. Nicole Sommer, PhD

und

Assoz.-Prof. Priv.-Doz. Dr. med. Annelie-Martina Weinberg

Graz, 01.04.2021

Eidesstattliche Erklärung

Ich erkläre ehrenwörtlich, dass ich die vorliegende Arbeit selbstständig und ohne fremde Hilfe verfasst habe, andere als die angegebenen Quellen nicht verwendet habe und die den benutzten Quellen wörtlich oder inhaltlich entnommenen Stellen als solche kenntlich gemacht habe.

Graz, am 01.04.2021 *Lisa Paar, eh.*

DANKSAGUNG

Ich möchte mich an dieser Stelle bei allen Menschen bedanken, die mir bei der Erstellung meiner Diplomarbeit zur Seite gestanden sind. Ein besonders großer Dank gilt meiner Betreuerin, Univ-Ass. Nicole Sommer, PhD, die mich während der gesamten Zeit optimal unterstützt hat und immer ein offenes Ohr für meine Fragen hatte. Weiters möchte ich mich sehr herzlich bei meiner betreuenden Professorin Assoz.-Prof. Priv.-Doz. Dr.med Annelie-Martina Weinberg bedanken.

CONTENTS

LIST OF ABBREVIATIONS

Mg	Magnesium
SD rats	Sprague Dawley rats
HA	Hydroxyapatite
PTH	parathyroid hormone
ESIN	elastic stable intramedullary nailing
Fe	Iron
Ti	Titanium
Zn	Zinc
Ca	Calcium
PLA	Polylactic acid
PGA	Polyglycol acid
PLGA	Polylactic glycol acid
TCP	Tricalcium phosphate
PTH	Parathyroid hormone
ZX00	Mg-0.45wt%Zn-0.45%wtCa

LIST OF FIGURES

LIST OF TABLES

ZUSAMMENFASSUNG

Hintergrund: In der pädiatrischen Orthopädie und Traumatologie hat die Osteosynthese als Mittel der Wahl zur Behandlung von Frakturen in den letzten Jahren zunehmend an Bedeutung gewonnen. Zur Frakturstabilisierung werden Materialien wie Titan, Stahl und weitere metallische Legierungen verwendet. Zurzeit ist es noch üblich, dass die eingesetzten Implantate bei Kindern wieder entfernt werden um etwaige Wachstumsbeeinträchtigungen bzw. metallische Präzipitationen zu vermeiden. Dies bedeutet wiederum, dass die pädiatrischen Patienten eine zweite Narkose und einen zweiten Krankenhausaufenthalt auf sich nehmen müssen. Materialien aus Magnesium (Mg) bzw. Mg-Legierungen liefern vielversprechende neue Ansätze in der Implantatentwicklung. Diese Materialien weisen sowohl eine exzellente Biokompatibilität, als auch geeignete mechanische Eigenschaften auf, um als Implantat zur Stabilisierung von Frakturen des wachsenden Knochens verwendet zu werden. Ein weiterer Vorteil von Magnesium-Implantaten ist ihre Eigenschaft, sich nach einer gewissen Zeitspanne vollständig aufzulösen, wodurch keine weitere Operation zur Entfernung des Implantats notwendig ist.

In dieser Studie untersuchten wir das Verhalten einer Mg-basierten Legierung (synthetisiert mit Zink und Kalzium; ZX00) im Kleintiermodell über einen Zeitraum von 24 Wochen.

Methoden: Für die bilaterale, transkortikale Implantation der zylindrischen ZX00 Pins in die proximale Metaphyse der Tibia wurden sieben weibliche, 6 Wochen alte Sprague Dawley (SD) Ratten verwendet. Als Kontrolle dienten drei SD Ratten, welche sich einer Sham-Operation (Bohrloch ohne Pin) unterzogen. Direkt nach der Operation und 2, 6, 12, 15, 18 und 24 Wochen nach der Operation wurden Mikro-CT Bilder der eingesetzten Implantate angefertigt und dreidimensional rekonstruiert. Mittels dieser Mikro-CT Bilder wurden das Implantatvolumen und -oberfläche, sowie die Wasserstoffgasbildung mit der Software MIMICS, Version 22 evaluiert.

Resultate: Die Ergebnisse zeigten eine gute Osseointegration und eine homogene Degradation mit adäquatem Gasvolumen. Trotz Implantation in direkter Nähe zur Wachstumsfuge wurde das Längenwachstum der Knochen nicht beeinträchtigt, welches durch das „Mitwachsen“ der Stifte über den gesamten Zeitraum von 24 Wochen gezeigt werden konnte.

Konklusion: Die Mg-Legierung ZX00 weist eine homogene Degradationsrate, moderate Wasserstoffgasbildung und eine gute Osseointegration ohne Beeinträchtigung der Knochenneubildung auf. ZX00 besitzt vielversprechendes Potential für den Einsatz als bioresorbierbaren Werkstoff in der Frakturstabilisierung in der Kinder- und Jugendorthopädie und -traumatologie, jedoch sind weitere Studien zur Evaluierung der Zugfestigkeit und Stabilität der Mg-Legierung, insbesondere in den ersten 6 bis 12 Wochen nach Osteosynthese notwendig.

ABSTRACT

Background: Osteosynthesis has significantly gained in relevance in pediatric orthopedics and traumatology over the last decades. Permanent metal implants like titanium, stainless steel and other metallic alloys are used for fracture treatment. Currently, implant removal is performed frequently in order to avoid possible long term side effects such as growth disturbance, discomfort or accumulation of corrosion products. Accordingly, another anesthesia and hospitalization is needed. New implant materials composed of magnesium (Mg) and Mg alloys exhibit promising features including excellent biocompatibility and mechanical properties meeting the demands for an enhanced fracture stabilizing implant in pediatric orthopedics and traumatology. Moreover, Mg-based implants dissolve after a certain period of time to their full extent, rendering a second surgery for implant removal unnecessary. In this study we investigated the *in vivo* degradation behavior of an Mg-based alloy synthesized with zinc and calcium (ZX00) in rats over a time period of 24 weeks.

Methods: Seven, female 6-weeks old Sprague Dawley rats underwent bilateral and transcortical implantation of cylindrical ZX00 pins into the proximal metaphysis of the tibia. Three Sprague Dawley rats underwent the same surgical intervention without implant, thereby serving as sham controls. To observe implant degradation and osseointegration, *in vivo* low-medium resolution micro-computed tomography was performed immediately after as well as 2, 6, 12, 15, 18 and 24 weeks after implantation. Images were three-dimensionally reconstructed and implant volume, implant surface and hydrogen gas formation was calculated using MIMICS Software, version 22.

Results: Our results showed a good osseointegration and homogenous degradation behavior of ZX00 with appropriate hydrogen gas formation. Although implants were inserted in close proximity to the growth plate, no negative effect on longitudinal bone growth could be observed.

Conclusion: We showed homogenous degradation, adequate gas evolution and good osseointegration of Mg-based ZX00 implants without bone growth determination. We conclude that ZX00 constitutes an appropriate biodegradable material for utilization in pediatric orthopedics and traumatology, however, further

studies are needed to prove rigidity of the material especially in the first six to twelve weeks of fracture healing.

1. INTRODUCTION

1.1. Anatomy and Morphology of Bone

The human skeleton is made up of 206 bones. Bone tissue and the skeletal system perform several basic functions in the human body, including support, protection, assistance in movement, mineral homeostasis, blood cell production and triglyceride storage.

Human bone is a complex and dynamic living tissue that is remodeled continuously. Each individual bone is an organ composed of different tissues: bone, cartilage, dense connective tissues, epithelium, blood-forming tissue, adipose tissue and nervous tissue.

All bones of the human skeleton are divided into five different categories based on their shape (1–3):

1) Long bones (lat. Ossa longa): The main characteristic of a long bone is that it is longer than it is wide. Long bones consist primarily of compact bone but may also have large amount of spongy bone at the ends or extremities (e.g. femur)
2) Short bones (lat. Ossa brevia): Short bones are cube-like in shape with vertical and horizontal dimensions approximately equal. They consist primarily of spongy bone, which is covered by a thin layer of compact bone (e.g. carpals of the wrist)
3) Flat bones (lat. Ossa plana): Flat bones are thin, flattened and usually curved (e.g. scapula)
4) Irregular bones (lat. Ossa irregularia): Irregular bones are usually of complex shape and do not fit in any other classification. They consist primarily of spongy bone that is covered with a thin layer of compact bone (e.g. vertebrae)
5) Sesamoid bones (lat. Ossa sesamoidea): Sesamoid bones are of small and round shaped and are embedded in tendons where a great deal of pressure is generated in a joint. The patellae is the largest and most well-known sesamoid bone.

To give a more detailed explanation on bone structure, long bones serve as the best example: a long bone is divided into epi- and diaphysis. Epiphysis is located at both ends of the bone. It consists of spongy bone, also called cancellous bone, which is

covered by a thin layer of compact cortical bone. In its cavity we find red marrow or myeloid tissue generating red blood cells, white blood cells and platelets. The long tubular shaft between the epiphysis is the diaphysis. The diaphysis consists of the medullary cavity filled with yellow marrow that is covered by a thin region of cancelleous bone and surrounded by a wall made of compact bone. Where diaphysis meets epiphysis, we find a narrow area, the metaphysis, that contains the epiphyseal plate (growth plate), which can only be found in a growing bone. When the bone stops growing, the cartilage is replaced by osseous tissue and the epiphyseal plate becomes the epiphyseal line (1,4).

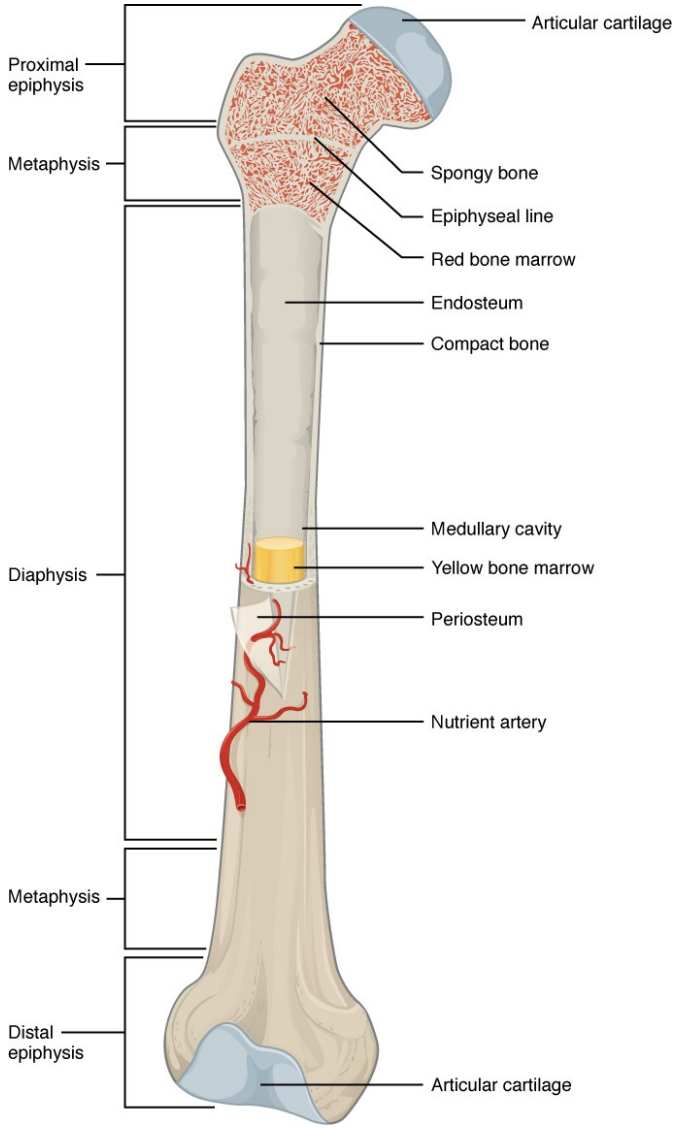

Figure 1: Anatomy of the long bone (1)

Proximal Epiphysis - Metaphysis - Diaphysis - Metaphysis- Distal Epiphysis

Epiphysis and Metaphysis consist of spongy bone and red bone marrow; the Diaphysis consists of compact bone and yellow bone marrow

At both extremities we find articular cartilage

Endosteum describes a layer of vascular connective tissue lining the medullary cavities of bone

Periosteum is a fibrous layer lining the surface of bone

1.2. Histology of Bone

Bone is a specialized dynamic tissue, consisting of calcified extracellular material, the bone matrix and the cellular part with three major cell types: osteocytes, osteoblasts and osteoclasts. Bone matrix consists of an inorganic component, crystals of calcium hydroxyapatite (HA) and an organic component, type I collagen. The HA crystals, mainly containing calcium and phosphorus, are arranged in ordered fashion along the type I collagen fibers, filling the gap regions and also the overlap regions. The surface of the HA crystals is hydrated, forming a hydration shell, which permits the exchange of ions between the mineral and body fluids. The collagen is arranged in large bundles, being highly cross-linked so it cannot be easily extracted. Most of the organic portion of bone matrix consists of type I collagen, but it also includes several glycoproteins, such as osteocalcin, osteopontin and osteonectin, being responsible for binding HA. Another matrix protein is bone sialoprotein, which has binding sites for bone matrix, osteoblasts and osteocytes.
The association of HA crystals and collagen provides the hardness and resistance of human bone. If bone is decalcified it retains its original shape but becomes soft and brittle and can be easily fractured (5–8).

Structurally and histologically bone can be divided into four main types: woven, lamellar, compact and cancellous bone. Woven bone is the nonlamellar immature bone which is formed during embryonal development and bone repair and is later replaced and organized as lamellar bone. Woven bone is characterized by irregular disposition of type I collagen fibers, a higher proportion of osteocytes and a lower mineral content than lamellar bone. Compact bone and cancellous bone both consist of lamellar bone. Lamellar bone is composed of multiple layers, so called lamellae, of calcified matrix, parallel or concentric arranged around a central canal. In each lamellae type I collagen fibers are alternating organized with the pitch of the fibers orientation shifting in a 90 degree angle in the successive lamellae. The main characteristic feature of lamellar bone are the osteons or haversian canal systems. An osteon is a complex of concentric lamellae arranged around a central canal, the haversian canal, which contains small blood vessels and a neurovascular bundle. Successive osteons are connected by Volkmann canals, areas which are formed due to preexisting blood vessels. Between adjacent lamellae osteocytes are

dispersed in lacunae, all connected by canaliculi allowing the exchange of nutrients, hormones, ions and waste products to and from osteocytes.

However, osteons can be subdivided into three additional types of lamellae: interstitial lamellae (remains of osteons), which have been partially absorbed by osteoclasts during growth and remodeling of bone; the external circumferential lamellae, which can be found just beneath periosteum and the inner circumferential lamellae, completely surrounding the marrow cavity (5–8).

1.2.1. Bone cells

Cellular components of bone tissue are divided in three main types and their pluripotent progenitor cells (5–7):

1) **Osteoblasts:** Under the influence of bone morphogenic protein-6 and transforming growth factor beta osteoprogenitor cells differentiate into osteoblasts. Osteoblasts are responsible for synthesis and secretion of the uncalcified organic component of bone matrix, the osteoid, including type I collagen fibers, glycoproteins and proteoglycans. Osteoblasts also possess several factors on their cell membrane, such as integrines and parathyroid hormone (PTH) receptors. When PTH binds to PTH receptors on the osteoblasts, receptor activator of NF-κB ligand (RANKL) is secreted.
2) **Osteocytes**: Osteocytes are former osteoblasts, situated in lacunae after being surrounded and trapped by calcified bone matrix. They form dendritic processes and communicate with each other via gap junctions. Between the lacunae, tunnel-like spaces, the canaliculi contain interstitial fluid to allow the exchange of metabolites and nutrients between osteocytes.
3) **Osteoclasts:** Osteoclasts develop from their progenitor cells with the help of two factors, macrophage colony-stimulating factor and RANKL, which are both produced by osteoblasts. Osteoclasts are responsible for enzymatic bone resorption, thereby being located in cavities on the bone surface, which are known as resorption lacunae or Howship lacunae.

1.3. Osteogenesis

Osteogenesis is the development of the bone. Bone is formed in two different ways: the intramembranous and the endochondral ossification. In both processes woven bone is produced first and is then replaced by lamellar bone. While in intramembranous ossification bone originates directly from mesenchyme, in endochondral ossification bone is formed over the intermediate step of a cartilage structure (5–7).

1.3.1. Intramembranous ossification

Intramembranous ossification takes place within mesenchymal connective tissue. During early ossification, primary ossification centers are highly vascularized and contain osteoprogenitor cells, which proliferate and differentiate into osteoblasts. Osteoblasts produce bone matrix that is continuously calcified, forming areas of woven bone. Between this forming network of trabeculae, the vascular connective tissue is transformed into bone marrow. Regions of mesenchymal tissue that do not undergo ossification become endosteum and periosteum of the bone (5–7).

1.3.2. Endochondral ossification

During endochondral ossification, bone is developed based on a cartilage template. This template consists of hyaline cartilage with vascularized perichondrium at its outsides. In this area osteoprogenitor cells differentiate into osteoblasts and the adjacent perichondrium becomes periosteum. Osteoblasts then start forming a subperiosteal bone collar on the surface of the cartilage model. As the bone collar keeps nutrients from diffusing to the hypertrophied chondrocytes, they eventually die, leaving empty confluent lacunae within the core of the cartilage template, which, later in process, becomes the medullary cavity. Osteoblasts further produce bone matrix and form a calcified cartilage-bone -complex. On the other hand osteoclasts resorb this complex, further enlarging the medullary cavity. Within this dynamic process, the epiphyseal growth plate is unaltered to continue its function during bone growth (5–7).

1.4. Epiphyseal growth plate

The epiphyseal plate or growth plate, consisting of epiphyseal cartilage, is responsible for longitudinal bone growth. At the epiphyseal side, chondrocytes proliferate and form cartilage, whereas, at the diaphyseal side, cartilage is continuously replaced by bone. The epiphyseal growth plate is histologically divided into five different zones (5–8):

1) Zone of reserve cartilage: This region is the zone closest to the epiphyseal end of the growth plate. It consists of hyaline cartilage and contains resting chondrocytes.
2) Zone of proliferation: In the zone of proliferation chondrocytes proliferate rapidly under the influence of a paracrine hormone called Indian hedgehog (produced by the chondrocytes) to influence all adjacent chondrocytes. While proliferating the chondrocytes are organized parallel to the long axis of the bone.
3) Zone of hypertrophy: In this zone terminally differentiated hypertrophic chondrocytes with accumulated glycogen in their cytoplasm are located. They synthesize and secrete vascular endothelial growth factor causing the invasion of blood vessels into the area.
4) Zone of calcification: Chondrocytes undergo apoptosis and cartilage matrix begins to calcify by forming hydroxyapatite crystals with calcium ions brought by invaded blood vessels.
5) Zone of ossification: Osteoprogenitor cells start to invade the area and differentiate into osteoblasts producing bone matrix which becomes calcified. As long as the rate of mitotic activity in the zone of proliferation equals the rate of resorption in the zone of ossification, the thickness of the epiphyseal growth remains the same and the bone continues to grow longer.

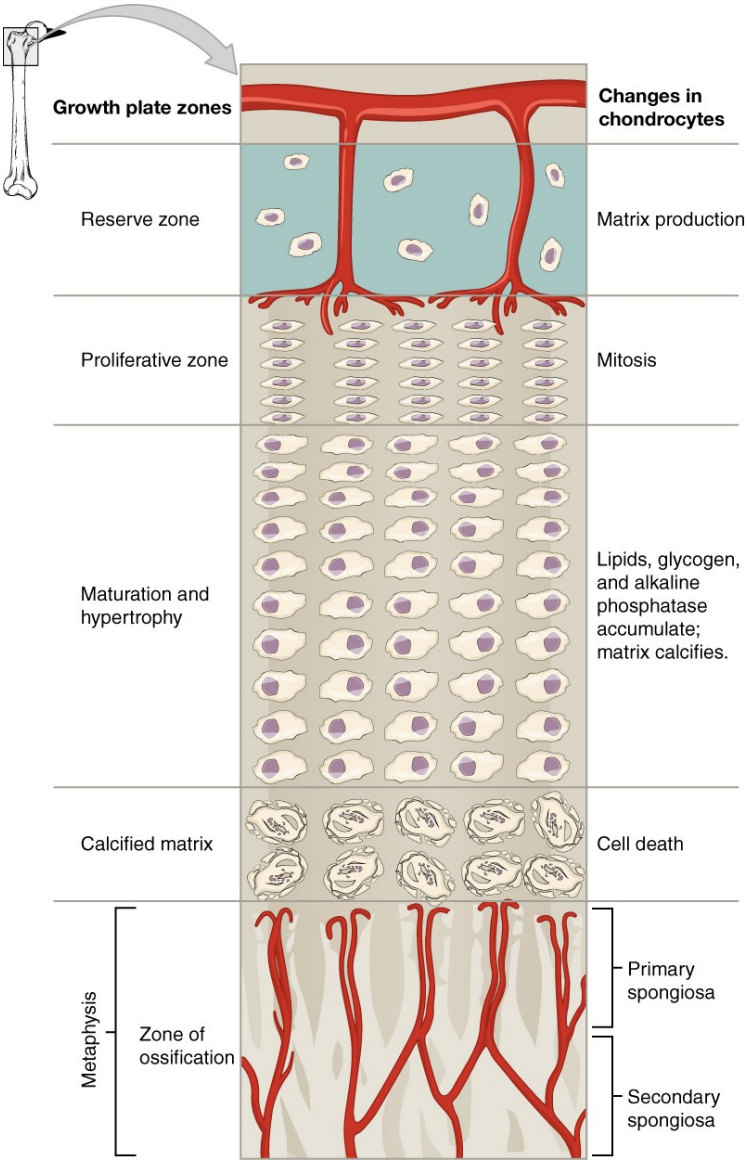

Figure 2: Histology of the epiphyseal growth plate (1)

The growth plate zones are subdivided according to cellular processes: In the reserve zone matrix production takes place; in the proliferation zone chondrocytes proliferate by mitosis; in the maturation and hypertrophy zone chondrocytes with accumulated lipids, glycogen and alkaline phosphatase are located; in the zone of calcification (calcified matrix) chondrocytes undergo apoptosis and cartilage matrix is calcified; in the zone of ossification osteoblasts produce bone matrix

1.5. Fractures

Bone fractures can be divided in complete or incomplete fractures, open or closed fractures as well as regarding the etiology in traumatic and not-traumatic fractures. Fractures lead to loss of strength, disturbance of blood supply, destruction of adjacent soft tissue and eventually loss of function in affected joints.

Concerning morphology, there are different types of fractures (9–17):

1) Transverse fracture: The break goes straight across the bone. Usually it is caused by a force applied from the fracture site.

2) Greenstick fracture: Greenstick fractures are characterized by an incomplete break of the bone. It usually occurs in younger children in mid-diaphyseal area, because their bones are less brittle and more bendable compared to adult bone. As force is applied on the bone, the convex site of the bone breaks, but the cortex of the concave site remains intact.
3) Spiral fracture: It occurs due to a twisting force applied to the bone.
4) Crush fracture: Crush fractures are commonly found in spongy bone. They are the result of forced compression of the bone.
5) Burst fracture: Burst fractures are fractures of the spine. The vertebral body is totally crushed and fragments of the bone might injure the spinal cord.
6) Avulsion fracture: A piece of fractured bone is torn away by a tendon or a ligament.
7) Stress fracture: Stress fractures are common among athletes. Bone breaks due to repeated stresses and strains applied to the bone.
8) Comminuted fracture: A comminuted fracture is a fracture where bone breaks in more than two fragments.
9) Intraarticular fracture: Fracture with involvement of a joint.
10) Fracture dislocation: Dislocation of a joint with a fracture in one of the bones of the joint.

1.5.1. Pediatric fractures

Compared to adult bone pediatric bone shows several differences. Due to a lower mineral and a higher water content, pediatric bone is more yielding and stronger in tension. As pediatric bones are still growing, the cartilaginous epiphyseal plate, which is responsible for longitudinal growth of bone is still existent. This area is predisposed for fractures and injuries, as it is weaker than bone. The periosteum of pediatric bone is much stronger, thicker and better vascularized compared to adult bone. Therefore, incomplete fractures (greenstick fractures or torus fractures) are more common in children (11,12,14,16).

Pediatric fractures of the epiphyseal growth plate are classified by Salter-Harris Types I to V and are further extended by the Ogden classification including

periphyseal fractures, which do not actually involve the epiphyseal growth plate but can also negatively influence the blood supply of the growth plate (14,15,17).

Salter Harris classification (14,15):

1) Salter Harris Type I: The fracture line goes straight through the epiphyseal plate. Zone of reserve cartilage and zone of proliferation are not involved. The diagnosis is based on clinical examination as X-ray imaging may be inconspicuous.
2) Salter Harris Type II: Transphyseal fracture involving the metaphysis. The fracture line goes through the epiphysis and, on one side of the bone, through the metaphysis. The metaphyseal fragment is called Thurston-Holland fragment.
3) Salter Harris Type III: Fracture through the epiphyseal plate exiting through the epiphysis. This type causes more troubles as the joint is involved and the zone of reserve cartilage and proliferation are likely to be damaged.
4) Salter Harris Type IV: The fracture line goes through the epiphysis, the epiphyseal plate and the metaphysis, disrupting all zones of the epiphyseal plate.
5) Salter Harris Type V: Epiphyseal plate is crushed by severe compression. All zones of the epiphyseal plate may be damaged.

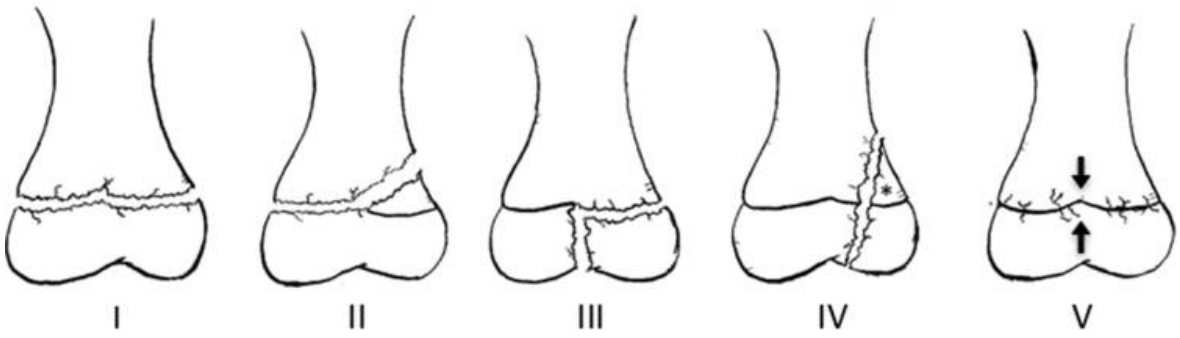

Figure 3: Salter-Harris classification of pediatric fractures (17)

Type I: straight fracture through the epiphyseal plate

Type II: transphyseal fracture involving the metaphysis

Typ III: fracture through the epiphyseal plate exiting through the epiphysis

Type IV: fracture through the epiphysis, epiphyseal growth plate and metaphysis

Type V: crush of the epiphyseal plate

1.5.2. Complications of pediatric fractures

Fractures of the epiphyseal plate may result in growth disturbances (depending on the fracture type, localisation and age of the patient), which can affect either parts or the entire epiphyseal plate and my lead to inequalities in length of the affected extremities, angular deformities and malpositions such as varus and valgus. They can be divided in two types: inhibiting and stimulative growth disturbances (18,19).

Inhibiting growth disorders result from a premature closure of the epiphyseal plate due to trauma, combustion, circulatory disturbance, immobilisation, infection or radiation. A complete closure is rare, more frequent is the partial premature closure of the epiphyseal plate of the lower extremities with formation of an osseous bridge due to consolidation in the area of the fracture gap (18–21).

Stimulative growth disturbances result either from hyperemia and local, humoral and hormonal reactions in vicinity of the fracture gap (complete stimulative growth disorder) or from remodelling processes in case of delayed compression of the fracture gap (partial stimulative growth disorder). Stimulation of the epiphyseal plate initially leads to lengthening of the affected extremity and subsequently to a shortening due to premature closure of the epiphyseal plate (18,19).

Another complication of pediatric fractures is osteonecrosis, resulting from the fact that the vascular system in children in some areas is not fully developed, which leads to insufficient blood supply and necrotic cell death (20,21).

1.6. Bone repair

Fractures in bone result in destruction of bone matrix and bone cells, disruption of periosteum and endosteum and formation of a localized hemorrhage filling in the zone of the fracture. There are two different ways of fracture healing: indirect fracture healing, which is the most common and natural process and direct fracture healing which requires an accurate adaption of the fracture ends and mechanical stabilization and fixation (15,16).

1.6.1. Indirect Fracture Healing

Bone repair is a multifunctional process, involving an acute inflammatory response, bone matrix and debris resorption, cartilage formation as well as intramembranous and endochondral bone formation.

Bone fractures are associated with damaged blood vessels that lead to the formation of a localized blood clot. The fracture initiates a proinflammatory response, which is essential for the healing process and is involved in recruitment of cells, promotion of angiogenesis, differentiation of mesenchymal stem cells, osteoblasts and osteoclasts. The most important signal molecules include tumor necrosis factor alpha, interleukin 1, 6, 11 and 18.
From the well vascularized periosteum, endosteum and the surrounding connective tissue capillaries and fibroblasts start to invade the blood clot forming granulation tissue. Osteoprogenitor cells differentiate into chondroblasts and produce cartilage. This process results in the formation of a soft fibrocartilaginous callus, covering the fracture ends of the bone. At the same time osteoprogenitor cells which did not differentiate into chondroblasts, but into osteoblasts, produce a hard collar of bone by intramembranous bone formation thus creating a combined collar of new bone and cartilage, the external callus. While the external callus grows continuously, the cartilage matrix is calcified, absorbed and gradually replaced with cancellous bone like in endochondral bone formation. Meanwhile osteoprogenitor cells and multipotential cells of the bone marrow have formed the internal callus in the marrow cavity. After the fracture ends are united by internal and external callus, the immature, woven bone of the callus is replaced by secondary or lamellar bone and the callus is resolved (15,16).

1.6.2. Direct fracture healing

There are two different types of direct fracture healing: contact and gap healing. The aim of contact healing it to close the fracture directly through re-establishment of Haversian systems. Therefore, contact healing requires an exact anatomic restoration of the fracture ends and rigid fixation. During gap healing, initial bone consisting of cancellous and lamellar bone is formed between the fracture ends, but

with transverse orientation to original bone. The second phase starts after several weeks with remodeling and formation of the Haversian systems in original orientation, finally building mechanically stable new bone (15,16).

1.7. General principles of pediatric fracture management

In terms of pediatric fracture treatment two general principles can be pointed out: the conservative approach with and without closed reduction and the operative management with closed or open reduction and fixation. General aims of pediatric fracture treatment includes the fast and effective pain relief, restoration of physiological anatomy and function with minimal necessary invasion, early mobilization and avoidance of secondary reduction attempts and late complications (22).

In contrast to adults pediatric bone possesses the ability of the so called spontaneous correction. This principle describes the ability of growing bone to adjust malrotations, axial malpositions and growth reductions spontaneously. It is usually possible up to 12 years of age or better until the physiological bone age is finished and the physis is almost closed. Spontaneous correction should always be taken under consideration in terms of pediatric fracture treatment (22,23).

1.7.1. Conservative management

Many pediatric fractures can be treated conservatively with and without closed reduction. Epiphyseal, metaphyseal and diaphyseal fractures without dislocation, epiphyseal fractures with only slight angular deviations and fractures of the clavicula in children under the age of 12 can be sufficiently treated conservatively with closed reduction and immobilization with plaster cast, fiberglass cast, splints or bandage. Repeated closed reduction should be avoided, in case of unsuccessful reposition or loss of reposition in the course of the healing process, secondary surgical treatment is indicated (18,22,23).

1.7.2. Surgical intervention

Surgical fracture treatment options include closed operative management and open reduction and fixation. Indications for surgical treatment include instable fractures, intraarticular fractures such as Salter Harris III and IV, open fractures and irreducible fractures in particular. Techniques used for closed reduction and open reduction and fixation are K-wires, cannulated screws, lag screw fixation, elastic stable intramedullary nailing (ESIN), intramedullary nailing, plate fixation and external fixation (22,23).

K-wires are used for closed or open reduced metaphyseal fractures and epiphyseal fractures of radius, femur or tibiae. They are inserted slowly close to the center of the physis and supplemented with cast or splint (22).

ESIN can be used for diaphyseal fractures in children 3 to 4 years before puberty with a maximum weight of 50 to 60kg. They cannot be administerd in treatment of intraarticular fractures (22).

Treatment of fractures involving the epiphyseal plate should include a follow-up two years afterwards or after skeletal growth has been completed in order to readjust potential malalignments (23).

1.8. Osteosynthesis of pediatric fractures

Before 1980, conservative procedures in treatment of pediatric fractures were mainly the method of choice. In 1983, French surgeons implemented a new way of fracture treatment by developing ESIN, which fulfilled the required properties for treatment of pediatric fractures and mainly replaced treatment with cast and immobilization. Over the time, osteosynthesis of pediatric fractures gained more and more importance, especially concerning unstable and dislocated fracture treatment (24–26).

The choice of appropriate materials for osteosynthesis plays a significant role in outcome and complication rate after treatment of pediatric fractures. Current state

of the art materials are non-resorbable implants made of titanium, stainless steel and other metallic alloys (27). With children titanium is commonly used as alloying system. Due to possible long term side effects of the remaining implant in children, such as growth disturbance, discomfort or accumulation of corrosion products, implant removal is usually performed (30-33). Accordingly, a second surgery with anesthesia and hospitalization is needed, which is associated with higher health care costs and risk of further complications (25,76). To overcome these issues, bioresorbable implants constitute an interesting alternative.

1.8.2. Bioresorbable and biocompatible Implants

Implantable devices have become indispensable in modern medicine, providing stupendous opportunities in diagnosis and therapy. After implantation they remain in the human body permanently or temporarily, supporting it, taking over functions or providing clinicians with valuable information. In orthopedics and traumatology medical implants are commonly used for osteosynthesis and therefore have to fulfill certain properties such as good biocompatibility and biofunctionality (25,34,35). In his paper of 2008 David F. Williams uses the following definition for biocompatibility: „Refers to the ability of a biomaterial to perform its desired function with respect to a medical therapy, without eliciting any undesirable local or systemic effects in the recipient or beneficiary of that therapy, but generating the most appropriate beneficial cellular or tissue response in that specific situation, and optimizing the clinically relevant performance of that therapy“ (36). In terms of pediatric orthopedics the medical implant has to meet certain requirements. The implant should exhibit high mechanical strength, while not lead to stress shielding due to a young´s modulus too high compared to human bone. It should not impede longitudinal bone growth, not release potential toxic particles and it should not provoke any local or systemic inflammatory and allergic reactions. Additionally, an ideal implant for bone fractures in children should be bioresorbable, making subsequent surgery for removal redundant (25,27). Several biodegradable materials have been under investigation over the last decades, but not all of them seem to be appropriate for fracture stabilization in children:

1) **Iron (Fe):** Fe and Fe alloys have shown several promising properties utilized as biodegradable implants in *in vivo* studies, such as high stability, a high tensile strength and a high load bearing capacity (37–39). Additionally, they did not provoke any local or systemic toxic and inflammatory reactions. Unfortunately, the degradation rate of Fe and also its of its alloys is relatively low mainly caused by the limited availability of oxygen in surrounding tissue, which is vital for Fe corrosion. The corrosion rate could also not be accelerated significantly by modifying alloy composition. Therefore, Fe and its alloys can be neglected in the choice of implant material for fracture stabilization in children (37–40).

2) **Zinc (Zn):** Zn-based alloys feature quite a low melting point, which means they can be processed applying simple procedures. However, low yield strength, tensile strength and plasticity of pure Zn represent a major impediment in using Zn as biodegradable implant material (25,39).

3) **Polymers:** Polymers offer a wide range of different types of materials and material composition. The most commonly used polymers for orthopedic applications are polyesters i.e. polylactic acid (PLA), polyglycol acid (PGA) and polylactic glycol acid (PLGA). Of all synthetic polymers polyesters are particularly attractive because of their degradation mechanism, hydrolysis of its ester bonds. Degradation rate can be altered as necessary by tailoring the chemical structure of polyesters, making them degrade slower or faster. The degradation products, lactic acid and glycolic acid, are considered to convert to carbon dioxide and water, finally being breathed out through the lungs. Another metabolic pathway is the conversion of glycolic acid into glyoxylate and further on into glycine. However, although the degradation products can be removed, tissue damage can be caused by an increase in local acidity. Further disadvantages of polymers in orthopedic application are the poor mechanical properties of sugar-derivated polymers. In comparison with biodegradable metals polymers facilitate a high brittleness and low strength and stiffness (25,41–44).

4) **Ceramics:** Biocompatible ceramic materials used in medical application are either bioinert, bioactive or bioresorbable. While bioinert ceramics are

characterized by their non-non-participation in chemical reactions and remain in the body unaffected, bioactive and bioresorbable implants interact with bone and tissue. Bioresorbable ceramics are composed of HA or tricalcium phosphate. HA offer excellent osteoconductivity and osteoinductivity, however, HA degrades far too slowly to be sufficiently used as bioresorbable implant in pediatric fracture treatment. Tricalcium phosphate (TCP), which is further divided by its crystallization in alpha and beta TCP, exhibit a more suitable degradation rate. Alpha TCP is cytotoxic und unstable, hence, of no use as implant material. Apart from its appropriate degradation rate, beta TCP also exhibit an osteoconductivity and osteoinductivity resembling those of HA. Therefore, beta TCP constitutes the most attractive choice as degradable biomedical implant compared to other ceramic compositions. A further positive aspect of TCP is its porous structure, promoting bone formation on implant surface and tissue ingrowth by providing sufficient nutrition supply. To outline some major disadvantages of bioceramics, their high brittleness and low tensile strength have to be mentioned, as limiting their usage in load-bearing applications (25,44,45).

1.8.3. Osseointegration, osteoconduction and osteoinduction

Demands towards medical implant materials are rising constantly. Thus, an optimal implant material ought not only be bioresorbable but also enable optimal bone growth on implant surface, described as osteoconduction and stimulate bone matrix producing cells, described as osteoinduction. Osteoconduction is dependent upon osteoinduction, as bone formation on a biomemetic interface can only take place with previous osteoinduction. Osteoinductive and osteoconductive abilities of materials vary widely, i.e. bone growth is not possible on copper and silver. Magnesium has been proven to be both osteoconductive and osteoinductive, hence, accelerating sustainable bone formation. To increase osteoconductive and osteoinductive abilities of less bioactive implant materials and thus create a biomimetic interface between implant and surrounding tissue, surface modification could be a promising option (42,46,47).

Osseointegration, osteoconduction and osteoinduction are common terms in scientific papers, however, not always used correctly. As Osteoconduction and osteoinduction can be shortly described as the interactions of bone cells with the implant surface, osseointegration is defined as „a direct - on light microscopic level - contact between living bone and implant“ (48). On a histological level osseointegration means direct contact between bone and implant due to bone formation around the implant without growth of connective tissue in between. On a biomechanical level, osseointegration is described by Zarb et al. as „a process whereby clinically asymptomatic rigid fixation of alloplastic materials is achieved, and maintained, in bone during functional loading“ (49).

In terms of bioresorbable implant development in pediatric orthopedics osseointegration of the implant is essential for a stable bone-implant interface and, consequently, optimal load bearing facilities and fracture healing.

1.9. Magnesium

1.9.1. The role of magnesium in the human body

Magnesium (Mg) is known to be the fourth most abundant cation occurring in the human body with an average total amount of 21g to 28g. About 50% of total Mg body content can be found in bone, about 50% is present in soft tissue and muscles with highest concentrations measured in liver and skeletal muscles. Only 1% of total Mg amount is found in extracellular fluid. The recommended daily allowance is about 350mg for male and 280mg for female with increasing demand during pregnancy and lactation (355mg). Mg is absorbed by the ileum and colon and excreted by the kidneys. In the kidney three quarter of total plasma Mg content is filtered in the primary urine and mainly reabsorbed in the thick ascending loop of Henle. 3-5% of filtered magnesium is finally excreted, which is about 60 to 120mg magnesium per day among normal adults. The kidney constitutes the main regulator of Mg homeostasis. The key hormones of Mg regulation include PTH, vitamin D and calcitonin, influencing Mg reabsorption in the kidney. Further it is reported that PTH causes Mg release from the bone and increased absorption in the intestine (50–52).

Mg is involved in a series of cellular functions and is indispensable for regular neurological and muscular function. As a cofactor in many enzymatic reactions, Mg modulates transport functions, protects biological membranes and is implicated in energy metabolism as well as in nucleic acid and protein synthesis. Mg deficiency mainly occur due to malnutrition, intestinal malabsorption, chronic pancreas insuffiency, alcoholism, diabetes, hyperaldosteronism and increased loss via enhanced renal excretion. Hence, Mg deficiency is associated with weakness, nausea, vomiting and lethargy and in a later stage can lead to paresthesia, muscle cramps, irritability and mental confusion (50).

In clinical aspects Mg compounded with sulfate is approved for prevention of eclamptic seizures in pregnancy and might also reduce the prevalence of cerebral palsy and mental retardation in premature infants. It has been reported that magnesium might have a neuroprotective effect on ischemic brain injury by blocking the NMDA receptor, increasing cerebral blood flow in the affected area, inhibiting Ca inflow into the cells and supporting cellular energy metabolism. Among patients with diabetes type 2 a constantly low cytosolic free magnesium level has been measured and it has been proven that Mg deficiency leads to increased insulin resistance. Supplementation of Mg has shown positive effects in terms of hypertension, atherosclerosis and asthma bronchiale, however further clinical studies are needed (50,53,54).

Mg consitutes a wide therapeutic margin and is commonly efficiently excreted via glomerular filtration, hence cases of severe Mg intoxication are barely described. Excessive oral Mg intake might cause mild intestinal symptoms (abdominal cramps, diarrhea). Intravenous injection of Mg can result in an increased level of free cytosolic Mg becoming noticable through vomiting, hypotension, cardiac arrhythmias, hyporeflexia, paralysis and in worst case respiratory and cardiac arrest (50,55).

Magnesium is a lightweight material showing several promising characteristics in terms of medical application in orthopedics and traumatology. With a density of 1.74 g/cm3, a Young´s modulus and yield strength close to human bone it has increasingly attracted attention in scientific research over the last years (25,27).

1.9.2. The role of magnesium as bioresorbable implant material

In children, permanent implants must be removed in many cases otherwise impeding longitudinal bone growth. Due to biodegradability, Mg and Mg alloys have gained major attention in pediatric orthopedic and trauma research, rendering a second removal surgery unnecessary. However, intensive research is needed to develop an implant material with a suitable degradation rate. Bioresorbable implants which dissolve too rapid do not allow satisfactory fracture healing and damage bone tissue by rapid corrosion and release of large amount of hydrogen gas. In recent years different Mg alloy compositions with various coatings and manufactural procedures were tested *in vitro* and *in vivo*. However, *in vitro* and *in vivo* degradation rates partially differ, thereby limiting reliable *in vitro* testing (56,57).

First application of Mg in orthopedics was described in 1932 when Lambotte stabilized fractures of the lower leg using Mg plates in combination with steel screws. However, due to extensive subcutaneous gas formation upon Mg corrosion, the implant had to be removed on the eighth day after implantation. The authors suggested an electrochemical reaction between Mg and steel (58,59). Furthermore, experiments with Mg plates in animal models and pure Mg nails in children demonstrated successful fracture treatment with degradation of Mg nails and no evidence of gas cavity formation (27,39).
In the 20th century, several animal experiments and clinical trials were conducted with pure Mg and Mg alloys and demonstrated positive effects on bone formation and fracture healing without causing severe inflammatory reactions (59,60). However, unpredictable corrosion behavior and incidental gas formation was observed (60–62). In order to improve corrosion resistance, Stroganov et al. synthesized Mg with cadmium (a rare earth element) to slow down the degradation rate (63). However, they made no reports about complications and long term effects of rare earth elements in the body. Witte et al. investigated the degradation behavior of Mg-aluminium alloys (AZ31, AZ91) and rare earth element containing Mg-alloys (WE43, LAE442) in an animal model by implanting sample rods in the femora of female guinea pigs. As a control, they used bioresorbable PLA implants. Animals with Mg-based implants showed increased bone formation compared to those with PLA implants. After one week, subcutaneous gas formation was observed, which was removed by a puncture procedure and gas formation was not further reported

in the upcoming weeks. Traces of rare earth elements could only be detected in the corrosion layer and not in the surrounding tissue. While LAE442 showed a slower degradation rate, degradation rate of the other materials were similar (64).

In another study, dynamic hip screws (DHS) made of bionic Ti and Mg were implanted into the proximal femur in humans. In comparison to the traditional Ti alloy and the bionic Ti alloy, the group demonstrated that bionic Mg DHS did not lead to stress shielding and loss of bone density and stability (27,65).
Additionally, several studies highlighted the good biocompatibility, osteoconductivity and osteoinductivity of Mg-based alloys as well as enhanced bone formation without provoking inflammatory reactions (24,66–69).

Antoniac et al. observed slow degradation rate of Mg-Zn-Mn alloys coated with hydroxyapatite (HAP) compared to uncoated Mg-Zn-Mn (70).
Marco et al. demonstrated the influence of the manufacturing process on Mg/Mg alloy degradation behavior associated with various impurity content and grain size (71).

Several in vivo studies investigating the Mg alloys ZX50 (Mg, Zn, Ca, Mn) and WZ21 (Mg, Zn, Ca, Mn, Y) showed that ZX50 degrades rapidly leading to a large amount of hydrogen gas formation around the implant. WZ21 degrades more slowly with a moderate release of hydrogen gas remaining constant over full time period showing that organism is capable of handling moderate gas production very well. Moreover, it could be shown that degradation behavior depends not only on the alloy composition but is also significantly influenced by implant site, as corrosion happens far more rapidly in the medullary cavity and slower in cortical bone areas due to increased metabolism and enhanced contact to blood vessels in the medullary cavity and tighter implant-bone junction in the cortex. Both materials allowed bone recovery restitutio ad integrum after complete implant degradation (66,72).
In a study investigated the influence of ZX50 and WZ21 on the epiphyseal growth plate, it could be shown that ZX50 impairs bone growth and shatters the epiphyseal plate significantly due to rapid degradation and hydrogen gas release while WZ21

degrades homogenously and more slowly leading only to minor damages on the growth plate and allowing full recovery (68).

Surface of ZX50 was treated with micro-arc oxidation in order to slow down degradation rate, however degradation rate proved to be even higher after week 3 post-implantation than in the untreated sample (67).

Although WZ21 proved to be superior to ZX50, it must not be neglected that WZ21 contains Yttrium, a rare earth element. Implant safety is of utmost importance in regards to pediatric application as not only short term but also long term undesirable side effects have to be ruled out. Amerstofer et al. detected Yttrium levels after 15 months in adjacent bone tissue, however there was no evidence of Yttrium accumulation after full implant degradation. Myrissa et al. evaluated implant degradation and distribution of rare earth elements in the organism after implanting Mg10Gd pins. Accumulation of gadolinium was observed in organs over whole degradation time with highest enrichment in the spleen (71,72).

With regard to implant safety Mg metabolism of generated Mg ions released from the dissolving implant has to be evaluated as well. Draxler et al. used isotopical enrichment of Mg to determine magnesium accumulation and excretion during implant degradation. The experiment showed that increased levels of Mg were mainly limited to implant surrounding tissue and only small quantities of magnesium could be found in organs with stable Mg serum values over the entire period of degradation. Isotopically enriched Mg from the implant was found in urine, indicating reliable renal excretion of incidental Mg derived from implant degradation. After complete degradation no implant derived Mg could be measured in bone tissue (73).

Grün et al. investigated degradation behavior and osseointegration of Mg implants composed of Mg, Zn and Ca (ZX00) in a small and large growing animal model and compared results with conventional titanium implants. ZX00 implants showed good osteoconductivity and osteoinductivity as it increased bone mass and established a strong bone-implant interface. It degraded slowly presuming total reabsorption after two years. Increased gas formation was observed but without impeding bone formation. As results of the study did not differ widely between the large and small animal model it was concluded that small animal models can be sufficiently applied for further investigations (69).

1.9.3. Degradation behavior of Mg

Pure Mg (99.9%) degrades with an acceleration of 10.5 - 210 mm per year under physiological conditions. In an aqueous solution Mg reacts with H_2O, generating Mg hydroxide (Mg(OH)) and hydrogen gas (H_2). Mg(OH) further binds with chloride ions, forming $MgCl_2$. While Mg hydroxide is fully insoluble and generates a protective layer on the surface of the implant, $MgCl_2$ is a soluble product, hence, can be transported and excreted (25,74).

Mg degradation is influenced by several factors as could be shown in several *in vitro* and *in vivo* investigations (66-69,83-89). As already mentioned above, Mg degradation depends on chlorid ions. Under *in vitro* conditions the chlorid ions concentration reaches an equilibrium during the corrosion process, thus, limiting further corrosion. *In vivo* a constant exchange between blood and surrounding tissue takes places, therefore an equilibrium of chlorid ions can never be reached and the corrosion process continues until full degradation of the implant (57). Another important factor regarding corrosion rate of Mg and Mg alloys is the pH value and the temperature of the surrounding environment. While an alkaline pH (> 11.5) initiates the formation of a hydroxide layer on the implants surface and thereby protects the implant from rapid corrosion, a lower pH value (under 11.5), such as found in *in vivo* conditions, enhance Mg corrosion (57,87). Regarding temperature, a study showed that the corrosion rate of a high-purity Mg at 37°C (body temperature) was twice as high as at 20°C (room temperature) (89). Proteins and amino acids also influence Mg degradation by forming a layer on the implant surface or by changing the extant corrosion layer. However, no unitary effect on corrosion rate could be determined, as protein content both decreased and increased the corrosion rate depending on alloy composition (57).

In vivo factors such as vascularization of surrounding tissue, water content and type of animal species must also be taken into consideration, however when comparing corrosion rates, changes in corrosion rate are only slight (57).

2. HYPOTHESIS AND AIM OF THE STUDY

Mg-based implants seem to be promising candidates to stabilize pediatric fractures due to excellent osseointegration, suitable mechanical properties and the ability to degrade over a certain period of time rendering a second surgery for implant removal unnecessary (25,47). However, degradation rate needs to be evaluated precisely as rapid degradation leads to disturbances in bone formation and destruction of the epiphyseal growth plate (66,68,72). Degradation rate depends primarily on implant material composition, manufacturing process and surface treatment (63,66,67,71,72). Moreover, bioresorbable implant degradation differs depending on the implantation site (66,72).

Based on preliminary studies in rat femur, the proposed study is based on the following hypotheses:

(i) the degradation rate of ZX00 is homogenous leading to adequate gas formation and osseointegration within a study duration of six months

(ii) the degradation rate in the metaphyseal area of the tibia is comparable to the degradation rate obtained after implantation into diaphysis of the femur

(iii) the transcortical implantation of ZX00 in the metaphyseal area of the proximal tibia does not impede longitudinal bone growth

To test our hypotheses, a lean Mg-based implant material (ZX00) synthesized with zinc (Zn) and calcium (Ca) Mg-zinc-calcium was transcortically implanted into the metaphyseal area of the proximal tibiae in rats. Here we investigated the most important parameters, including implant volume, implant surface and gas volume using *in vivo* micro-computed tomography, to assess the degradation behavior of ZX00.

3. MATERIAL AND METHODS

3.1. Ethical statement

Small animal studies were approved by the Austrian Federal Ministry for Science and Research and followed the guidelines on accommodation and care of animals formulated by the European Convention for the Protection of Vertebrate Animals Used for Experimental and Other Scientific Purposes (GZ number: BMWFW-66.010/0124-WF/V/3b/2015). According to the 3R principles (replace, reduce and refine), all animal experiments were carried out to minimize suffering.

3.2 Material development

The purified Mg was alloyed with Zn and Ca to synthesize the alloy Mg-0.45 wt%Zn-0.45 wt%Ca. After solution and aging heat-treatments, indirect extrusion was performed at 325 C. Subsequently, pins were machined using polycrystalline diamond tools, taking special care to avoid any kind of surface contamination. Pins were then cleaned using ultrasonic waves, air dried in clean-room atmosphere and packaged airtight. Sterilization was performed by gamma irradiation (minimum dose 25 kGray).

3.3. Animals and surgery

Four-weeks-old, female Sprague Dawley (SD) rats (n = 10) were purchased from Janvier Labs (Saint Berthevin, France) and kept on normal chow for the entire study. All rats were housed in a conventional facility, which maintained a 12-hour light/dark cycle with free access to food and water. At six weeks of age, seven SD rats underwent bilateral, transcortical and proximal implantation of cylindrical ZX00 implants (two implants per rat; 14 implants in total) into the metaphysis of the tibiae. Three SD rats underwent the same surgical intervention without implant, thereby serving as sham controls.

3.3.1. Anesthesia

Volatile isoflurane (Forane®, Abbot AG, Baar, Switzerland) was administered for general anesthesia preceded by a subcutaneous combined sedation, administering a mixture of Fentanyl (20 µg kg−1 Fentanyl®, Janssen-Cilag GmbH, Neuss, Germany), Midazolam (400 µg kg−1 Midazolam Delta®, DeltaSelect GmbH, Dreieich, Germany) and Medetomidine (200 µg kg−1 Domitor®, Pfizer Corporation Austria GmbH, Vienna, Austria).

3.3.2. Transcortical implantation

Both hind legs were shaved, antisepticized with alcohol pads, and dried. A skin incision (length, 1-2 cm) was made medial over the proximal lateral tibial metaphysis, cleared from blood and connective tissue. A drill (1.55 mm) with ascending diameter (Synthes, Paoli, PA, USA) was used to prepare the bicortical implantation bed. Drilling was performed at a low rotational speed of 200 rpm and profuse physiological saline irrigation was applied using a syringe in order to minimize frictional heat and thermal necrosis. The cylindrical implant (l=8 mm, d= 1.6 mm) was inserted by gentle tapping, resulting in a uniform press fit. After transcortical placement was ensured, the operating field was irrigated thoroughly with physiological saline solution and the wound was closed. Postoperatively all animals received 200 mg kg1 Caprofen (Rimadyl, Pfizer Corporation, Vienna, Austria), which was injected subcutaneously on the day of operation to ensure analgesia. During the first postoperative week (up to the seventh day) analgesia maintained by administration of 60 mg Piritramid (Dipidolor; Janssen-Cilag GmbH, Neuss, Germany) in 40 ml 5% glucose added to 500 ml drinking water. Postoperatively, the rats were allowed to move freely in their cages without external support and unrestricted weight bearing. Daily clinical observation was performed throughout the study period.

3.3.3. Euthanasia

Twenty-four weeks after transcortical implantation, rats were euthanized with 25 mg sodium thiopental (Thiopental® Sandoz, Sandoz GmbH, Kundl, Austria) by injection into the cardiac ventricle leading to immediate cardiac arrest (79). All tibiae were explanted and kept at -80 °C for further investigation.

3.4. In vivo low-medium resolution micro-computed tomography (µCT)

In vivo µCT(Siemens Inveon µCT device) scans were performed 2, 6, 12, 15, 18 and 24 weeks after surgical intervention (n = 10) at a resolution of 56 µm per voxel. The scan data were converted into DICOM format and imported into the medical image processing software Mimics (Version 22.0, Materialise, Leuven, Belgium). Three-dimensional (3D) morphometric analysis was performed and implant volume and surface as well as gas and bone volume were assessed. At each µCT time point, animal weight was observed and any deviations were recorded.

3.5. Quantification of implant degradation parameters

Quantification of the implant degradation behavior was performed via Mimics Software, version 22.0.
In order to evaluate each tibia individually, orientation of all planes was assessed via function „Image- Reslice Images“ in order to illustrate the implant in all three planes and in all layers, the longitudinal and transversal axes of the implant served as main indicators.

3.5.1. Quantification of implant volume and surface

Via function „Segment - New Mask“ with a threshold of 226 to 3071 Hounsfield Units, a mask was placed on the images in order to separate implant from bone. As the prescribed thresholds of Hounsfield Units did not cover bone and implant in all µCT images, the threshold values of Hounsfield Units had to be adjusted individually. Via function „Segment - Split Mask“ µCT images could be separated in two masks, the Mg implant and rats bone (Figure 4). As the division of the mask was partially implemented imprecisely, a manual post-processing in all planes had to be conducted in order to ensure an accurate calculation of the implant volume and surface values. Subsequently, a three-dimensional (3D) model of the implant was constructed via function „Mask - Calculate Part“ and volume (in $mm^{3)}$ and surface (in $mm^{2)}$ values were evaluated (Figure 4).

3.6. Quantification of gas volume

Quantification of the generated hydrogen gas volume was performed via creating a second mask with „Segment - New Mask“ with Hounsfield Units of -1000 to -1024. The threshold values were again modified individually in order to ensure a precise measurement of the entire gas volume. Via function „Mask - Calculate Part“ a 3D model of the gas volume was constructed and the gas volume in mm3 was calculated (Figure 4).

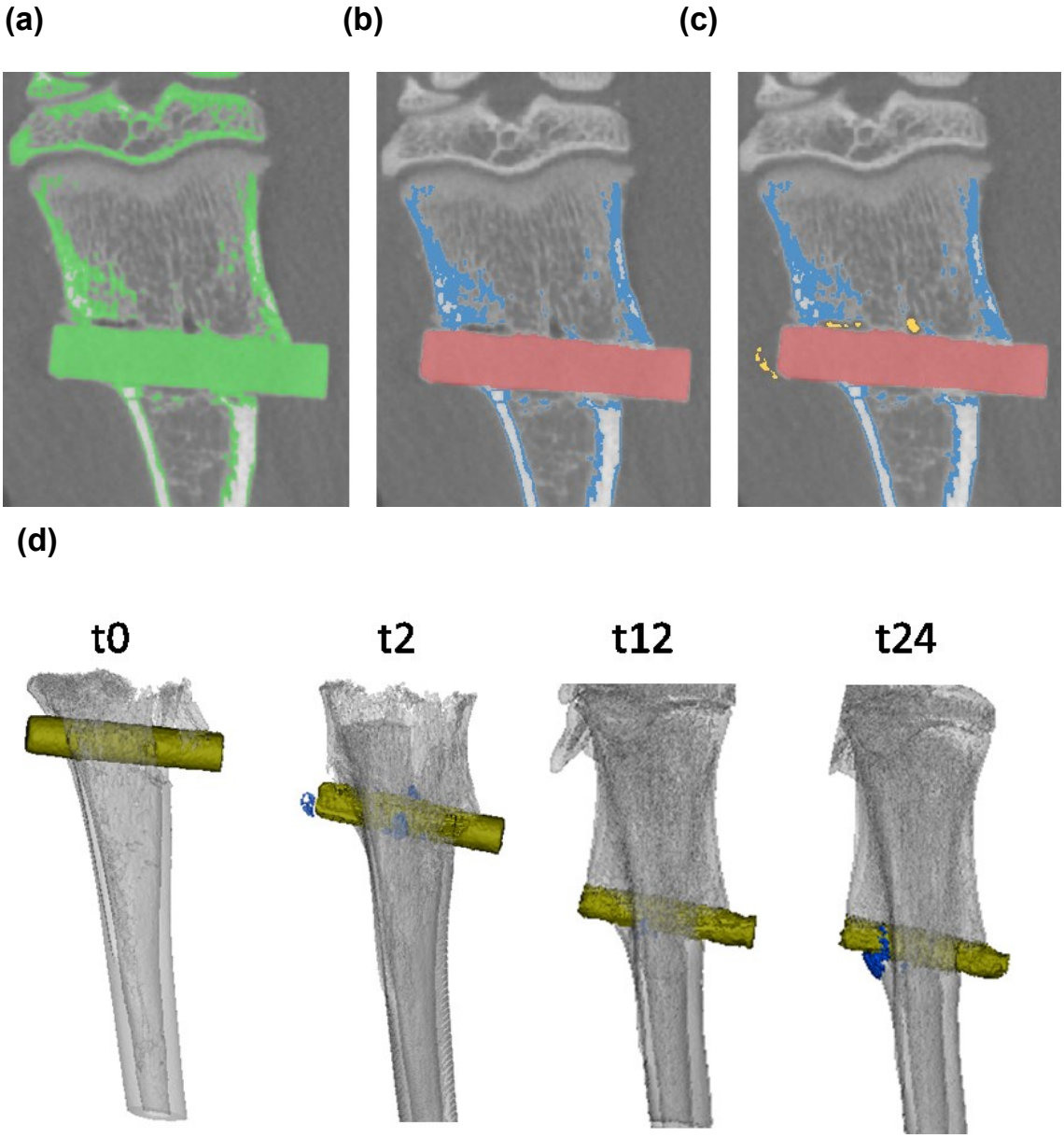

Figure 4: Segmentation of µCT image data via gray value orientated region growing algorithm: *In vivo* µCT scans were performed immediately after as well as 2, 6, 12, 15, 18 and 24 weeks after implantation. To evaluate implant volume and surface, as well as gas volume, µCT images were resliced and underwent quantification via Mimics Software. (a) Bone and ZX00 implant show comparable HU units, therefore (b) individual segmentation was performed; (c) after adding a new mask, which assessed dark spots, gas evolution was quantified; (d) example of 3D reconstruction of ZX00 pins

3.7. Quantification of degradation rate

In order to quantify the implants degradation rate RV in mm/day of µm/day following formula was used:

$$R_V = \frac{\Delta V}{<S>\ \Delta t},$$

Delta V (in mm^3) is the difference between the average implant volume value of time point 6 and time point 12, delta t is the time span between time point 6 and time point 12 in days (42 days). <S> (in mm^2) was assessed via calculating the average implant surface value between time point 6 and 12.

3.8. Statistical analysis

In order to compare results with literature, they are given as mean ± standard deviation (SD), although the rat sample number was below 10. Implants volume, surface and hydrogen gas volume were assessed via one-way ANOVA. A p-value < 0.05 was considered statistically significant.

4. RESULTS

Female 6-weeks old SD rats underwent transcortical implantation in the proximal metaphysis of both tibiae using cylindrical ZX00 pins (n=7) or served as sham controls (n=3), respectively. *In vivo* low-medium resolution µCT scans were performed immediately after surgery (time point 0) as well as 2, 6, 12, 15, 18 and 24 weeks after implantation. Moreover, bodyweight was measured at all µCT time points.

During the entire study period of 24 weeks, the bodyweight of all SD rats increased in all animals (Figure 5). In order to investigate whether ZX00 implantation had any impact on bodyweight gain compared to sham operated animals, bodyweight data was collected and compared by mean and standard deviation. The data demonstrates that implantation with ZX00 did not influence bodyweight gain compared to sham group over the entire study period of 24 weeks (Figure 5). For instance, after 24 weeks there was no significant difference in bodyweight between SD rats implanted with ZX00 (370.17 g ± 27.59 g) and the sham operated group (374.33 g ± 26.76 g) (Table 1). Therefore, we suggest that ZX00 implantation had no severe effect on eating behavior or on physical activity of the SD rats.

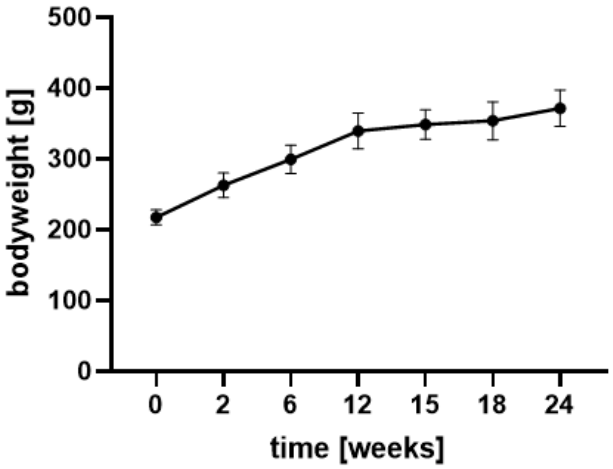

Figure 5: Bodyweight gain over the entire study period of 24 weeks. After ZX00 implantation bodyweight was measured at each µCT time point including 0 (immediately after implantation), 2, 6, 12, 15, 18 and 24 weeks. Data is shown as mean ± standard deviation (SD).

Table 1: Bodyweight corresponding to the individual rat and time point: Bodyweight (in g) of SD rats was measured immediately before as well as 2, 6, 12, 15, 18 and 24 weeks after implantation. For each time point, mean and standard deviation (mean ± SD) were calculated, comparing rats with and without pin implantation.

Rat no.	Impl/sham	BW=0	BW=2	BW=6	BW=12	BW=15	BW=18	BW=24
1	ZX00	207	265	299	342	340	357	368
2	ZX00	238	291	340	384	386	410	416
3	ZX00	226	266	307	335	343	361	374
4	ZX00	200	237	271	306		318	334
5	ZX00	220	281	310	372	370	373	377
6	Sham	218	259	290	324	331	331	350
7	ZX00	210	235	272	309	322	327	352
8	ZX00	213	256	293	332	343	350	
9	Sham	220	269	311	332	337	343	370
10	Sham	222	268	301	358	366	368	403
	Mean ZX00	216.29	261.57	298.86	340	350.67	356.57	370.17
	SD ZX00	12.79	20.88	23.86	29.35	23.13	30.41	27.59
	Mean sham	220	265.33	300.67	338	344.67	347.33	374.33
	SD sham	2	5.51	10.5	17.78	18.72	18.88	26.76

4.1. ZX00 shows good osseointegration without negatively influencing longitudinal bone growth

Osseointegration describes the integration of an implant within bony tissue, generating a stable bone-implant interface. In this study, *in vivo* µCT scans were performed to observe osseointegration of ZX00 pins (l=8mm, d=1.6mm) within the proximal metaphysis of the tibiae over a time period of 24 weeks. Therefore, different time points were chosen including time point 0 (immediately after implantation) as well as 2, 6, 12, 15, 18 and 24 weeks after surgery. In total, seven

rats underwent ZX00 implantation in the left and right tibiae, respectively, leaving 14 implants for investigation. At time point 0, air inclusions occurring due to the implantation process could be observed, creating a gap between bony tissue and implant material. During the course of the study, formation of a tight network between adjacent bony tissue and implant surface could be observed, indicating good osseointegration of ZX00 pins (Figure 6). Micro-CT images also showed that longitudinal bone growth of the juvenile rats remained unaffected by ZX00 pin implantation throughout the entire study period (Figure 6).

Figure 6: In vivo observation of ZX00 degradation over 24 weeks. ZX00 (Mg-0.45wt%Zn-0.45%wtCa) cylindrical pins were transcortically inserted into the proximal metaphysis of the left (upper panel) and right (lower panel) tibia of 6-weeks old SD rats. Degradation behavior, bone growth and osseointegration were observed immediately after surgery as well as 2, 6, 12, 15, 18 and 24 weeks post-implantationem.

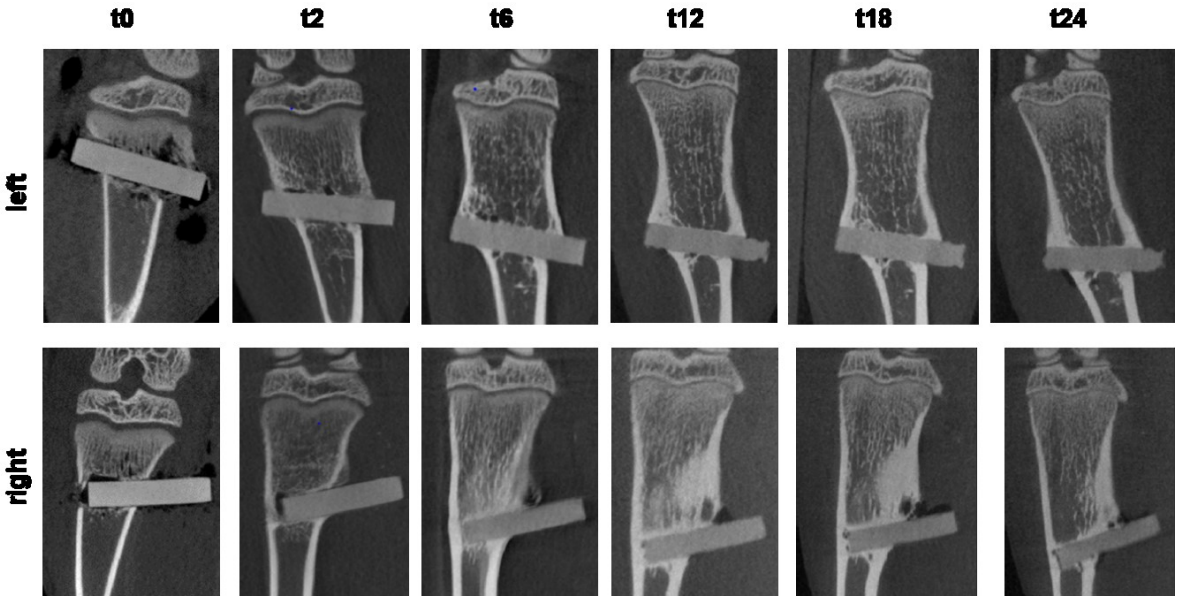

4.2. Degradation behavior of ZX00 implants evaluated via calculation of implant volume and implant surface alteration

Evaluation of the implant degradation behavior was performed via calculation of volume differences of the implant in Mimics Software, Version 22.0 (Table 2). In total, 14 implants were measured at seven different time points (time point 0, 2, 6, 12, 15, 18 and 24). The initial volume of the ZX00 pins (time point 0) was measured with an average value of 16.39 mm^3. Two weeks after implantation a mean increase in volume of the ZX00 to an average implant volume value of 17.04 mm^3 (3.9% relative increase) could be observed. Six weeks after implantation there was a slight increase to 17.14 mm^3 (0.6% relative increase) compared to week 2. Twelve weeks after implantation, the implant volume (16.45 mm^3) decreased approximately to the initial volume value (16.39 mm^3) (Figure 7). Eighteen weeks after implantation, the implant volume significantly decreased to an average value of 14.693 mm^3 (relative decrease of 10.3%) compared to the initial pin volume (time point 0). At the end of the study, 24 weeks after implantation, a total loss in volume with an average value of 13.926 mm^3 (15% relative loss in volume), was evaluated.

Table 2: Descriptive analysis of mean volume values of all ZX00 implants. Seven SD rats underwent bilateral, transcortical implantation of ZX00 pins (sample size = 14). Implant volume was calculated at seven different time points over a whole time period of 24 weeks. Micro-CT images were processed via MIMICS Software, version 22.

Implant volume in mm^3		
Week	**Mean Volume**	**Standard deviation**
0	16.386	0.561
2	17.036	0.734
6	17.139	1.772
12	16.454	2.901
15	15.133	0.847
18	14.693	1.174
24	13.928	1.274

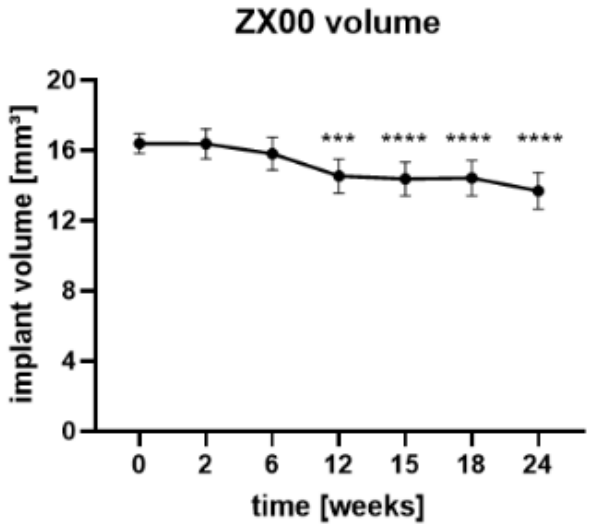

Figure 7: Implant volume alteration over the entire study period of 24 weeks: evaluation of all implant volume values of all implants inserted in the left and right rats tibiae at seven different time points (0, 2, 6, 12, 15, 18 and 24 weeks after implantation). Data is shown as mean ± standard deviation (SD).

Additionally, implant surfaces were analyzed at designated µCT time points (Table 3).

Table 3: Descriptive analysis of mean surface values of all ZX00 implants. Seven SD rats underwent bilateral, transcortical implantation of ZX00 pins (sample size = 14). Implant surface was calculated at seven different time points over a whole time period of 24 weeks. Micro-CT images were processed via MIMICS Software, version 22.

Implant surface in mm²		
Week	**Mean Surface**	**Standard deviation**
0	47.436	1.891
2	53.956	4.314
6	60.199	3.323
12	60.733	3.555
15	61.901	5.001
18	54.909	4.016
24	57.718	5.645

Immediately after surgery, at time point 0, the surface of the ZX00 implants was measured with an average value of 47.44 mm^2 (Table 3). Two weeks after implantation the implant significantly increased to an absolute value of 53.96 mm^2

(13.74% relative increase) compared to the initial pin surface (Figure 8). Furthermore, six weeks after surgery, the surface area significantly increased to an absolute value of 60.20 mm^2 (26.91% relative increase compared to the initial surface value). However, over the time period of the next two points of measurement (time point 12 and 15), only marginal surface alterations could be observed. At time point 18, the average surface value reached 54.91 mm^2 (15.75% decrease compared to time point 0). After the entire period of surface measurements, 24 weeks after implantation, the average surface value amounts to 57.71 mm^2, 21.66% relative increase compared to initial surface value.

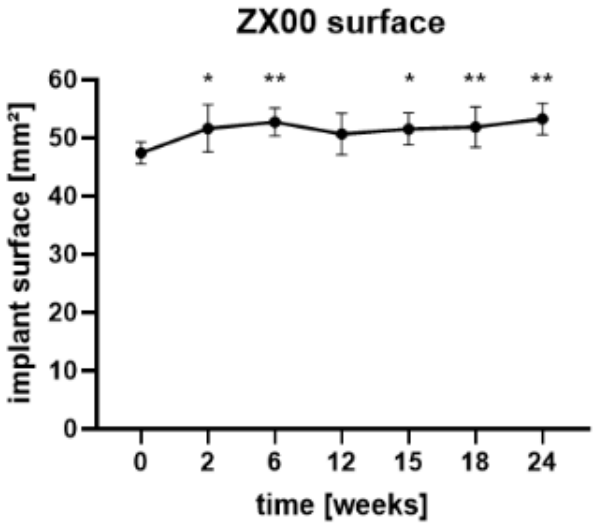

Figure 8: Implant surface alteration over the entire study period of 24 weeks: evaluation of implant surface values of all implants inserted in the left and right rats tibiae at seven different time points (0, 2, 6, 12, 15, 18 and 24 weeks after implantation). Data is shown as mean ± standard deviation (SD).

Table 4: Surface-to-volume ratios of all ZX00 implants at seven different time points over 24 weeks shown as mean ± standard deviation (SD).

Surface-to-volume ratios in mm^{-1}		
Week	**Mean**	**Standard deviation**
0	2.9	0.12
2	3.12	0.24
6	3.56	0.5
12	3.76	0.48
15	4.12	0.47
18	3.75	0.32
24	4.16	0.41

Surface-to-volume ratios of ZX00 increased only slightly with from originally 2.9 mm^{-1} to 3.76 mm^{-1} after 12 weeks and to 4.16 mm^{-1} after 24 weeks indicating moderate degradation without formation of severe corrosion spots (Table 4).

In order to compare ZX00 degradation with literature, degradation rate per day RV was assessed using differences in implant´s average volume and surface between time point 6 and 12 (used as representatives). The degradation rate was calculated with 0.51µm per day, assuming an average degradation rate of 186.15µm per year.

4.3. Evaluation of hydrogen gas formation in vicinity of ZX00 implant

Upon material degradation, hydrogen gas is released. In order to evaluate the hydrogen evolution over 24 weeks, *in vivo* low-medium resolution µCT imaging was performed. Three-dimensional reconstruction of ZX00 implants and hydrogen gas pockets were assessed by Mimics Software, version 22. Hydrogen gas volume was measured at six different time points over an entire time period of 24 weeks, starting with first measurement at time point 2, two weeks after surgical implantation (Table 5). At time point 2 the mean value of hydrogen gas volume was measured with 2.87 mm^3. Six weeks after implantation an increase in hydrogen gas volume could be observed with an average value of 4.795 mm^3 (67,3% relative increase). At this time point highest hydrogen gas levels were measured. In the further course of the study, gas evolution minimized, reaching an average value of only 1.589 mm^3 24 weeks after implantation. Gas evolution was shown to be more pronounced in cortical bone areas (Figure 6).

Table 5: Descriptive analysis of mean gas volume values of all ZX00 implants.
Seven SD rats underwent bilateral, transcortical implantation of ZX00 pins (sample size = 14). Hydrogen gas volume was evaluated at seven different time points over a whole time period of 24 weeks. Micro-CT images were processed via MIMICS software, version 22.

Gas volume in mm^3		
Week	**Mean Volume**	**Standard deviation**
0		
2	2.866	3.466
6	4.795	10.276
12	1.719	2.943
15	2.126	4.153
18	1.676	2.581
24	1.589	1.529

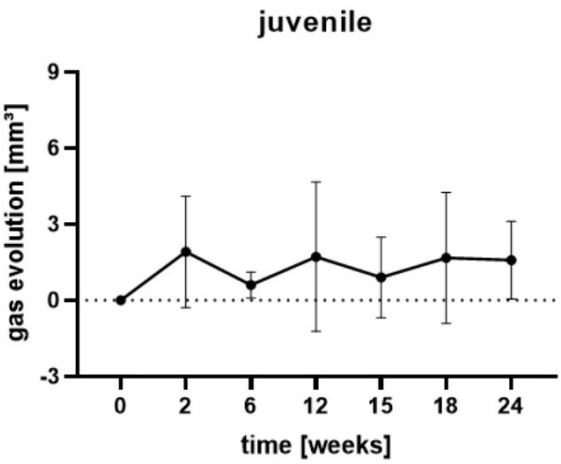

Figure 9: Hydrogen gas evolution over the entire study period of 24 weeks: evaluation of gas volume, generated by implant degradation, after insertion in the left and right tibia of SD rats at six different time points (2, 6, 12, 15, 18 and 24 weeks after implantation). Data is shown as mean ± standard deviation (SD).

5. DISCUSSION

In the recent years, conservative treatment strategies in pediatric fracture treatment have mainly been replaced by osteosynthesis procedures to reduce hospital length of stay and associated health care costs and psychological strain for children and parents (25). However, with this change in treatment strategy new issues have to be faced to ensure the best possible outcome. Osteosynthesis describes the surgical procedure of reuniting two or more bone fragments after proper reposition by means of screws, pins, plates and other fracture stabilizing devices (25,75). In order to achieve sufficient fracture healing, the choice of the applied implant material plays a major role as it should support bone healing process properly by providing the required mechanical stability and showing good osteoconductivity and osteoinductivity to promote bone formation.

At the current time, titanium alloys represent the „gold standard“ in pediatric fracture treatment (25,28). Titanium is a rigid material, showing good load-bearing capacities, however, due to a Young´s Modulus too high compared to human bone, it may lead to „stress shielding“ and reduced bone formation and density (28,29). As titanium is a non-resorbable implant, implant removal is commonly performed in children to avoid possible growth disturbance, discomfort and accumulation of corrosion products (30-33). Every surgery stresses the body and is an additional risk factor for occurrence of intra- and postoperative complications, such as bleeding and infection. What must also not be neglected is the risk of the general anesthesia under which osteosynthesis in children is commonly performed. Hypoxia, laryngeal injuries, pulmonary baro- and volutrauma and allergic reactions can occur as complications of airway management, mechanical ventilation and administered anaesthetics (76).

Implant materials which are not only biocompatible, osteoinductive and load bearing but also resolve after a certain period of time, hence, rendering a second surgery unnecessary, constitute an interesting alternative to conventional materials.

The usage of Mg as implant material is indeed not an entirely new approach, as it has been topic of investigation since beginning of the 20th century (27,39,58–62). However, unpredictable degradation behavior and major hydrogen gas formation have long limited its application in orthopedic surgery. In recent years, research focused again on the development of a Mg-based alloys with the aim of producing

a lightweight, biocompatible material, which dissolves homogenously, stabilizing the fracture as long as mechanical support is needed. In children, mechanical strength of the implant should be be maintained to full extent for a time span of at least 4 weeks (77). Several studies have been conducted, investigating various Mg-based alloys in different compositions, with and without surface modification in order to achieve more information about degradation behavior, osseointegration, gas formation, accumulation of degradation products, impact on juvenile bone growth and general tolerance i.e. no inducement of systemic inflammatory reactions (24,64,66–72). A very promising composition proved to be the alloy WZ21, a Mg-based material synthesized with the rare earth element yttrium. Yttrium improves the mechanical stability of Mg and increases corrosion resistance effectively (78). Kraus et al. investigated this alloy in terms of corrosion behavior, hydrogen gas formation and impact on the epiphyseal plate in a small animal model. They showed that WZ21 degrades with moderate speed, only slight gas formation and without impairing the epiphyseal plate and bone growth significantly, especially compared to another Mg alloy (ZX50) without addition of rare earth elements (68). However, a major limitation in the use of alloys with rare earth elements in pediatric orthopedics is the unknown long-term of effects due to their accumulation in organs, a fact which is utterly important in pediatric surgery due to the long post-operative lifespan of the patients (66,68). Consequently, attempts were made to develop a biodegradable Mg alloy facilitating stable mechanical properties, moderate degradation behavior and manageable gas formation free from any potential toxic contents (69). In a study performed by Grün et al. the Mg alloy ZX00 composed of pure Mg, Zn and Ca showed promising results in terms of degradation behavior and gas formation. It degrades homogenously with a volume loss of 19% after 24 weeks presuming total reabsorption after 2.5 years. Increased gas formation was observed but without impeding bone formation. Additionally, ZX00 implants showed good osteoconductivity and osteoinductivity as it increased bone mass and established a strong bone-implant interface (69).

In our study, ZX00 pins were implanted into the proximal metaphysis of the tibiae in a small growing animal model. In vivo low-medium resolution µCT scans were performed immediately after as well as 2, 6, 12, 15, 18 and 24 weeks after implantation. Implant volume and surface as well as hydrogen gas formation were

calculated via Mimics Software, version 22. Additionally, degradation behavior, osseointegration and impact of material degradation on the juvenile bone were assessed. Previous studies showed a significant good concordance between µCT images and histological thin slides and highlighted excellent reproducibility and analysis possibilities of µCT imaging performed on living animals, thus for evaluation of degradation behavior, osseointegration and bone formation in our study µCT constitutes the only method of choice (66).

In this study we demonstrated that transcortical implantation of cylindrical ZX00 pins into the proximal metaphysis of the tibia results in homogenous degradation with adequate gas evolution without disturbing longitudinal bone growth. From week 12th on, the implant volume significantly decreased, thereby indicating good stability, load-bearing capacity and homogenous degradation behavior. In comparison to other Mg-based implants, such as ZX50 or WZ21, ZX00 exhibited a lower degradation rate (68). While ZX50 corroded rapidly with a complete degradation already after 12 weeks, WZ21 degraded much slower. Twenty-four weeks after surgery, 48% and 53% of the initial pin volume were remaining. However, after 24 weeks, 85% of the initial ZX00 implant volume were detectable. As both studies were established on a small animal model and size and shape of the implants corresponded mostly, corrosion rates can be compared validly and divergences in corrosion rate are reasoned with variation in Mg alloy composition. The initial increase in ZX00 implant volume can be explained due to the successful osseointegration of the implant and formation of a corrosion layer within the first upcoming weeks, which made the distinction between implant and bone more complicated. Witte et al. described this corrosion layer as a newly formed mineral phase consisting mainly of calcium and phosphorous which is generated under Mg alloy degradation process and bone implant interaction. They suggested that this corrosion layer of calcium phosphates and Mg hydroxides and oxides plays a major role in slowing down the alloy degradation (64).

The surface of the inserted ZX00 implants significantly increased two weeks after surgery. However, after 12 weeks there was no difference in implant surface detectable, whereas after 15, 18 and 24 weeks, ZX00 implant surface significantly increased compared to the initial surface value. The initial increase of the ZX00 surface can be explained by the formation of a corrosion layer and the beginning of

implant degradation, which results in fraying of the implant´s surface and consequently leads to surface enlargement. Moreover, we demonstrated the moderate increase of surface-to-volume ratio from 2.9 mm^{-1} at time point 0 to 3.76 mm^{-1} after 12 weeks; and to 4.16 mm^{-1} after 24 weeks. These results indicate homogenous degradation without forming massive localized corrosion attacks. Studies with the Mg alloys ZX50 and WZ21, ZX50 showed a decrease in surface from the beginning and a very high surface-to-volume ratio (4.13 mm^{-1} to 24.47 mm^{-1} after 12 weeks) due to its rapid corrosion. WZ21 exhibited an increase in surface comparable with ZX00, however, surface increase was significantly higher compared to ZX00 with a surface growth of about 250% of initial surface value after 12 weeks. Surface-to-volume ratio of WZ21 was calculated with 3.37 mm^{-1} at the begin of the study and increased to 11.58 mm^{-1} after 12 weeks, indicating a more moderate degradation compared to ZX50 and faster degradation compared to ZX00 (68).

Mg dissolves under physiological conditions according to the reaction $Mg + H_2O \Rightarrow Mg(OH)_2 + H_2$ (66). Mg hydroxide ($Mg(OH)_2$) is insoluble, hence, coating the implants surface and protecting it from further corrosion. In a second electrochemical reaction, Mg binds to chloride, forming soluble $MgCl_2$, which is transported and excreted (25). During Mg degradation, hydrogen gas is released, which is detectable as gas bubbles in the vicinity of the implant by µCT. Upon ZX00 degradation, moderate hydrogen gas formation was observed during the entire study period. Hydrogen gas formation showed a peak after 6, 12 and 18 weeks, which levelled out until week 24. These results are comparable with the study of Grün et al., which showed a more pronounced gas evolution after 12 and 18 weeks after implantation in the diaphysis of the femur of juvenile, growing SD rats (69). In general, gas formation was more pronounced within the trabecular structure compared to compact bone. However, we also observed hydrogen gas evolution in the surrounding tissue, which is mainly caused by stress corrosion (69). Stress corrosion develops when forces are applied on protruding implant parts. For instance, due to the movement of the anima, muscle can apply forces onto the implant leading to stress that results on higher degradation rates. However, stress corrosion does usually not occur in humans, since screws are not oversized when compared to the rat model. Here, we calculated a degradation rate of 186.15µm per year (0.18 mm/year), which is comparable to degradation values of other different

Mg-based implant materials in literature which range from 0.25 mm/year to 1.45 mm/year (79,80). However, calculations of the ZX00 degradation rate after implantation in the diaphysis of the femur revealed a degradation value of 0.08 mm/year (69). The difference in degradation rates can only be explained by the different implantation site. In previous studies it has already been reported that degradation rate is dependent upon implantation site as degradation rate was higher in the epiphyseal than in metaphyseal/diaphyseal area, which was attributed to increased perfusion (68,81). As metaphyseal and epiphyseal blood supply are directly connected it can be assumed that metaphyseal perfusion is also higher compared to diaphyseal perfusion (81). Additionally, it is known that metaphyseal periosteum is higher in thickness and cell number compared to diaphyseal periosteum, which is also likely to contribute to differences in degradation behavior (82).

However, the homogenous degradation rate and adequate gas evolution can be attributed to the high-purity of the employed ZX00 alloy.

Grün et al. showed a strong osseointegration of ZX00 pins in a growing rat model contemporarily after implantation, increasing slightly over the conducted study period of 24 weeks. Additionally, they observed enhanced bone formation in operated rats compared to sham controls without implant, which can be explained by small bone lesions caused through the implantation process and mechanical stress post-operative (69). In this study, osseointegration of ZX00 was less evident in the beginning of the study due to initial hydrogen gas formation around the implant. However, osseointegration improved even after six weeks. Furthermore, we demonstrated that hydrogen gas formation did not impair bone in-growth and bone remodeling comparable to other studies (69). Adverse effects of hydrogen gas on juvenile bone growth and osseointegration of the implant, which were described in some studies, could not be observed (39,68).

6. CONCLUSIO

In conclusion, we demonstrated that ZX00 overcomes the disadvantages associated with state-of-the art permanent metal implants by demonstrating homogenous degradation, adequate gas evolution and good osseointegration without showing adverse effects on bone growth due the proximity of the implantation site to the epiphyseal plate. Hence, further studies are needed to prove the rigidity of the ZX00 implant material especially in the first six to twelve weeks until fractures are generally healed. These results give hope to path the way for a healthy Mg implant material into the operation theater of pediatric orthopedics and traumatology.

7. REFERENCES

1. Anatomy and Physiology - OpenStax [Internet]. [zitiert 25. Dezember 2020]. Verfügbar unter: https://openstax.org/details/anatomy-and-physiology

2. Classification of Bones | SEER Training [Internet]. [zitiert 25. Dezember 2020]. Verfügbar unter: https://training.seer.cancer.gov/anatomy/skeletal/classification.html

3. Anton Waldeyer; Friedrich Anderhuber; Franz Pera; Johannes Streicher. Waldeyer Anatomie des Menschen. 19. Auflage. De Gruyter; 2012. 1195 S.

4. Henry Gray, Henry Vandyke Carter, Warren H. Lewis. Anatomy of the human body. Philadelphia: Lea & Febiger; 1918.

5. Anthony L. Mescher. Junqueira´s Basic Histology: Text and Atlas. 15th Edition. McGraw-Hill Education Ltd; 1136 S.

6. Leslie P. Gartner. Textbook of Histology. 4th Edition. Elsevier LTD, Oxford; 2016. 672 S.

7. Michelle Peckham. Histology at a Glance. 1st Edition. John Wiley & Sons Inc; 2011. 112 S.

8. Renate Lüllmann-Rauch; Esther Asan. Taschenlehrbuch Histologie. 6. Auflage. Thieme; 2019. 784 S.

9. T. Duckworth; C.M. Blundell. Orthopaedics and Fractures. 4th Edition. Chicester: Wiley-Blackwell (an imprint of John Wiley & Sons Ltd); 2010.

10. Kenneth A. Egol, Kenneth J. Koval, Joseph D. Zuckerman. Handbook of Fractures. 5th Edition. Lippincott Williams&Wilki; 2014. 896 S.

11. Sammy Alexander Baierlein. Frakturklassifikationen. 1st Edition. Thieme; 2010. 240 S.

12. Radswiki. Greenstick fracture | Radiology Reference Article | Radiopaedia.org [Internet]. Radiopaedia. [zitiert 25. Dezember 2020]. Verfügbar unter: https://radiopaedia.org/articles/greenstick-fracture

13. Kalfas I, MD. Burst Fractures: Defined and Diagnosed [Internet]. SpineUniverse. [zitiert 25. Dezember 2020]. Verfügbar unter: https://www.spineuniverse.com/conditions/spinal-fractures/burst-fractures-defined-diagnosed

14. Harry B. Skinner, Patrick J. McMahon. Current diagnosis & treatment in orthopedics. 5th Edition. New York: McGraw Hill Education/Medical; 2014. (McGraw-Hill´s AccessMedicine).

15. Marsell R, Einhorn TA. The biology of fracture healing. Injury. 1. Juni 2011;42(6):551–5.

16. Jay R. Lieberman, Gary E. Friedlaender. Bone Regeneration and Repair: Biology and Clinical Applications. Softcover reprint of hardcover 1st ed. 2005. Humana Press; 2010. 410 S.

17. Cepela DJ, Tartaglione JP, Dooley TP, Patel PN. Classifications In Brief: Salter-Harris Classification of Pediatric Physeal Fractures. Clin Orthop. November 2016;474(11):2531–7.

18. Breitfuss H, Weinberg A-M, Muhr G. Wachstumsphänomene bei Frakturen im Kindesalter: Spontankorrekturen und Wachstumsstörungen. In: Weinberg A-M, Tscherne H, Herausgeber. Tscherne Unfallchirurgie: Unfallchirurgie im Kindesalter 2 Untere Extremität Körperhöhlen Besonderheiten des kindlichen Skelettes [Internet]. Berlin, Heidelberg: Springer; 2006 [zitiert 25. Dezember 2020]. S. 39–49. Verfügbar unter: https://doi.org/10.1007/3-540-36006-9_3

19. Hasler CC, von Laer L. Pathophysiologie posttraumatischer Deformitäten der unteren Extremität im Wachstumsalter. Orthop. 1. September 2000;29(9):757–65.

20. Carl Joachim Wirth, Wolf-Eberhard Mutschler, Johann Neu. Komplikationen Kompakt: Orthopädie und Unfallchirurgie. 1. Auflage. Thieme; 2015. 240 S.

21. Rodríguez-Merchán EC. Pediatric Fractures of the Forearm. Clin Orthop Relat Res. März 2005;432:65–72.

22. Epomedicine. General Principles - Pediatric Fracture Management [Internet]. Epomedicine. 2020 [zitiert 25. Dezember 2020]. Verfügbar unter: https://epomedicine.com/medical-students/principles-pediatric-fracture-management/

23. Annelie-Martina Weinberg, Harald Tscherne. Tscherne Unfallchirurgie: Unfallchirurgie im Kindesalter - Teil 1: Allgemeiner Teil, Kopf, Obere Extremität - Teil 2: Untere Extremität, Wirbelsäule, Körperhöhlen, Besonderheiten des kindlichen Skelettes. 1. Auflage. Berlin, Heidelberg: Springer; 2006.

24. Pichler K, Kraus T, Martinelli E, Sadoghi P, Musumeci G, Uggowitzer PJ, u. a. Cellular reactions to biodegradable magnesium alloys on human growth plate chondrocytes and osteoblasts. Int Orthop. April 2014;38(4):881–9.

25. Grün NG, Holweg PL, Donohue N, Klestil T, Weinberg A-M. Resorbable implants in pediatric fracture treatment. Innov Surg Sci. 29. Mai 2018;3(2):119–25.

26. Ligier JN, Metaizeau JP, Prévot J. [Closed flexible medullary nailing in pediatric traumatology]. Chir Pediatr. 1983;24(6):383–5.

27. Staiger MP, Pietak AM, Huadmai J, Dias G. Magnesium and its alloys as orthopedic biomaterials: A review. Biomaterials. 1. März 2006;27(9):1728–34.

28. Niinomi M, Nakai M. Titanium-Based Biomaterials for Preventing Stress Shielding between Implant Devices and Bone. Int J Biomater. 2011;2011:836587.

29. Frost HM. Wolff's Law and bone's structural adaptations to mechanical usage: an overview for clinicians. Angle Orthod. 1. Juni 1994;64(3):175–88.

30. Peterson HA. Metallic Implant Removal in Children. Journal of Pediatric Orthopaedics. Februar 2005;25(1):107.

31. Reith G, Schmitz-Greven V, Hensel KO, Schneider MM, Tinschmann T, Bouillon B, u. a. Metal implant removal: benefits and drawbacks--a patient survey. BMC Surg. 7. August 2015;15:96.

32. Asri RIM, Harun WSW, Samykano M, Lah N a. C, Ghani S a. C, Tarlochan F, u. a. Corrosion and surface modification on biocompatible metals: A review. Mater Sci Eng C Mater Biol Appl. 1. August 2017;77:1261–74.

33. Boulos A, DeFroda SF, Kleiner JE, Thomas N, Gil JA, Cruz AI Jr. Inpatient orthopaedic hardware removal in children: A cross-Sectional study. J Clin Orthop Trauma. 2017;8(3):270-275. doi:10.1016/j.jcot.2017.06.020

34. Li J, Stachowski M, Zhang Z. 11 - Application of responsive polymers in implantable medical devices and biosensors. In: Zhang Z, Herausgeber. Switchable and Responsive Surfaces and Materials for Biomedical Applications [Internet]. Oxford: Woodhead Publishing; 2015 [zitiert 25. Dezember 2020]. S. 259–98. Verfügbar unter: http://www.sciencedirect.com/science/article/pii/B9780857097132000110

35. Ahmed W, Elhissi A a, Jackson MJ a, Ahmed E b. Precision machining of medical devices [Internet]. The Design and Manufacture of Medical Devices. Elsevier Ltd; 2012 [zitiert 25. Dezember 2020]. Verfügbar unter: https://www.scopus.com/inward/record.uri?eid=2-s2.0-84904138012&doi=10.1016%2fB978-1-907568-72-5.50002-9&partnerID=40&md5=f2ee9b57b79cc279acc4d008fc846d7f

36. Williams DF. On the mechanisms of biocompatibility. Biomaterials. Juli 2008;29(20):2941–53.

37. Kraus T, Moszner F, Fischerauer S, Fiedler M, Martinelli E, Eichler J, u. a. Biodegradable Fe-based alloys for use in osteosynthesis: Outcome of an in vivo study after 52weeks. Acta Biomater. 1. Juli 2014;10(7):3346–53.

38. Purnama A, Hermawan H, Couet J, Mantovani D. Assessing the biocompatibility of degradable metallic materials: State-of-the-art and focus on the potential of genetic regulation. Acta Biomater. 1. Mai 2010;6(5):1800–7.

39. Pogorielov M, Husak E, Solodivnik A, Zhdanov S. Magnesium-based biodegradable alloys: Degradation, application, and alloying elements. Interv Med Appl Sci. März 2017;9(1):27–38.

40. Hofstetter J, Martinelli E, Pogatscher S, Schmutz P, Povoden-Karadeniz E, Weinberg AM, u. a. Influence of trace impurities on the in vitro and in vivo degradation of biodegradable Mg–5Zn–0.3Ca alloys. Acta Biomater. 1. September 2015;23:347–53.

41. Gunatillake PA, Adhikari R. Biodegradable synthetic polymers for tissue engineering. Eur Cell Mater. 20. Mai 2003;5:1–16; discussion 16.

42. Gentile P, Chiono V, Carmagnola I, Hatton PV. An overview of poly(lactic-co-glycolic) acid (PLGA)-based biomaterials for bone tissue engineering. Int J Mol Sci. 28. Februar 2014;15(3):3640–59.

43. Agrawal CM. Biodegradable Polymers for Orthopaedic Applications. In: Reis RL, Cohn D, Herausgeber. Polymer Based Systems on Tissue Engineering, Replacement and Regeneration [Internet]. Dordrecht: Springer Netherlands; 2002 [zitiert 25. Dezember 2020]. S. 25–36. (NATO Science Series). Verfügbar unter: https://doi.org/10.1007/978-94-010-0305-6_3

44. Godavitarne C, Robertson A, Peters J, Rogers B. Biodegradable materials. Orthop Trauma. 1. Oktober 2017;31(5):316–20.

45. Ceramics in Arthroplasty, Arthritis and Orthopaedics. 1:4.

46. Albrektsson T, Johansson C. Osteoinduction, osteoconduction and osseointegration. Eur Spine J Off Publ Eur Spine Soc Eur Spinal Deform Soc Eur Sect Cerv Spine Res Soc. Oktober 2001;10 Suppl 2:S96-101.

47. Bohlen J, Meyer S, Wiese B, Luthringer-Feyerabend BJC, Willumeit-Römer R, Letzig D. Alloying and Processing Effects on the Microstructure, Mechanical Properties, and Degradation Behavior of Extruded Magnesium Alloys Containing Calcium, Cerium, or Silver. Materials. Jänner 2020;13(2):391.

48. Albrektsson T, Brånemark P-I, Hansson H-A, Lindström J. Osseointegrated Titanium Implants: Requirements for Ensuring a Long-Lasting, Direct Bone-to-Implant Anchorage in Man. Acta Orthop Scand. 1. Jänner 1981;52(2):155–70.

49. Albrektsson T, Brunski J, Wennerberg A. „A requiem for the periodontal ligament“ revisited. Int J Prosthodont. April 2009;22(2):120–2.

50. Saris NE, Mervaala E, Karppanen H, Khawaja JA, Lewenstam A. Magnesium. An update on physiological, clinical and analytical aspects. Clin Chim Acta Int J Clin Chem. April 2000;294(1–2):1–26.

51. Wacker WEC, Parisi AF. Magnesium Metabolism [Internet]. http://dx.doi.org/10.1056/NEJM196803282781306. Massachusetts Medical Society; 2010 [zitiert 25. Dezember 2020]. Verfügbar unter: https://www.nejm.org/doi/pdf/10.1056/NEJM196803282781306

52. Okuma T. Magnesium and bone strength. Nutr Burbank Los Angel Cty Calif. August 2001;17(7–8):679–80.

53. Caddell J, Graziani L, Wiswell T, Hsieh H, Mansmann HC. The possible role of magnesium in protection of premature infants from neurological syndromes and visual impairments and a review of survival of magnesium-exposed premature infants. Magnes Res. 1999;

54. Muir K. Magnesium in stroke treatment. Postgrad Med J. 1. Dezember 2002;78:641–5.

55. J. Larry Jameson, Anthony Fauci, Dennis Kasper, Stephen Hauser, Dan Longo. Harrison´s Principles of Internal Medicine. 20th Edition. McGraw-Hill Education Ltd; 2018. 4400 S.

56. Myrissa A, Agha NA, Lu Y, Martinelli E, Eichler J, Szakács G, u. a. In vitro and in vivo comparison of binary Mg alloys and pure Mg. Mater Sci Eng C. 1. April 2016;61:865–74.

57. Sanchez AHM, Luthringer BJC, Feyerabend F, Willumeit R. Mg and Mg alloys: How comparable are in vitro and in vivo corrosion rates? A review. Acta Biomater. 1. Februar 2015;13:16–31.

58. A. Lambotte. L´utilisation du magnesium comme materiel perdu sans l´osteosynthèse. Bull Mém Soc Nat Chir. 1932;

59. J. Verbrugge. L´utilisation du magnèsium dans le traitement chirurgical des fractures. Bull Mém Soc Nat Chir. 1937;

60. ED. McBride. Magnesium screw and nail transfixion in fractures. South Med J. 1938;

61. McBRIDE ED. ABSORBABLE METAL IN BONE SURGERY: A FURTHER REPORT ON THE USE OF MAGNESIUM ALLOYS. J Am Med Assoc. 31. Dezember 1938;111(27):2464–7.

62. Maier O. Über die Verwendbarkeit von Leichtmetallen in der Chirurgie (metallisches Magnesium als Reizmittel zur Knochenneubildung). Dtsch Z Für Chir. 1. Mai 1940;253(8):552–6.

63. Stroganov GB, Savitsky EM, Tikhova NM, Terekhova VF, Volkov MV, Sivash KM, u. a. Magnesium-base alloy for use in bone surgery [Internet]. US3687135A, 1972 [zitiert 25. Dezember 2020]. Verfügbar unter: https://patents.google.com/patent/US3687135A/en

64. Witte F, Kaese V, Haferkamp H, Switzer E, Meyer-Lindenberg A, Wirth CJ, u. a. In vivo corrosion of four magnesium alloys and the associated bone response. Biomaterials. 1. Juni 2005;26(17):3557–63.

65. Cun Y, Dou C, Tian S, Li M, Zhu Y, Cheng X, u. a. Traditional and bionic dynamic hip screw fixation for the treatment of intertrochanteric fracture: a finite element analysis. Int Orthop. 1. März 2020;44(3):551–9.

66. Kraus T, Fischerauer SF, Hänzi AC, Uggowitzer PJ, Löffler JF, Weinberg AM. Magnesium alloys for temporary implants in osteosynthesis: In vivo studies of their degradation and interaction with bone. Acta Biomater. 1. März 2012;8(3):1230–8.

67. Fischerauer SF, Kraus T, Wu X, Tangl S, Sorantin E, Hänzi AC, u. a. In vivo degradation performance of micro-arc-oxidized magnesium implants: A micro-CT study in rats. Acta Biomater. 1. Februar 2013;9(2):5411–20.

68. Kraus T, Fischerauer S, Treichler S, Martinelli E, Eichler J, Myrissa A, u. a. The influence of biodegradable magnesium implants on the growth plate. Acta Biomater. 15. Jänner 2018;66:109–17.

69. Grün NG, Holweg P, Tangl S, Eichler J, Berger L, van den Beucken JJJP, u. a. Comparison of a resorbable magnesium implant in small and large growing-animal models. Acta Biomater. 15. September 2018;78:378–86.

70. Antoniac I, Miculescu F, Cotrut C, Ficai A, Rau JV, Grosu E, u. a. Controlling the Degradation Rate of Biodegradable Mg–Zn-Mn Alloys for Orthopedic Applications by Electrophoretic Deposition of Hydroxyapatite Coating. Materials. Jänner 2020;13(2):263.

71. Myrissa A, Braeuer S, Martinelli E, Willumeit-Römer R, Goessler W, Weinberg AM. Gadolinium accumulation in organs of Sprague–Dawley® rats after implantation of a biodegradable magnesium-gadolinium alloy. Acta Biomater. 15. Jänner 2017;48:521–9.

72. Amerstorfer F, Fischerauer SF, Fischer L, Eichler J, Draxler J, Zitek A, u. a. Long-term in vivo degradation behavior and near-implant distribution of resorbed elements for magnesium alloys WZ21 and ZX50. Acta Biomater. 15. September 2016;42:440–50.

73. Draxler J, Martinelli E, Weinberg AM, Zitek A, Irrgeher J, Meischel M, u. a. The potential of isotopically enriched magnesium to study bone implant degradation in vivo. Acta Biomater. 15. März 2017;51:526–36.

74. Miller PL, Shaw BA, Wendt RG, Moshier WC. Assessing the Corrosion Resistance of Nonequilibrium Magnesium-Yttrium Alloys. Corrosion. 1. Dezember 1995;51(12):922–31.

75. Merolli A. 13 - Using bone repair materials in orthopaedic surgery. In: Planell JA, Best SM, Lacroix D, Merolli A, Herausgeber. Bone Repair Biomaterials [Internet]. Woodhead Publishing; 2009 [zitiert 25. Dezember 2020]. S. 349–77. (Woodhead Publishing Series in Biomaterials). Verfügbar unter: http://www.sciencedirect.com/science/article/pii/B9781845693855500131

76. De Francisci G, Papasidero AE, Spinazzola G, Galante D, Caruselli M, Pedrotti D, u. a. Update on complications in pediatric anesthesia. Pediatr Rep [Internet]. 18. Februar 2013 [zitiert 25. Dezember 2020];5(1). Verfügbar unter: https://www.ncbi.nlm.nih.gov/pmc/articles/PMC3649741/

77. Wilkins KE. Principles of fracture remodeling in children. Injury. Februar 2005;36 Suppl 1:A3-11.

78. Liu X, Shan D, Song Y, Han E. Influence of yttrium element on the corrosion behaviors of Mg–Y binary magnesium alloy. J Magnes Alloys. 1. März 2017;5(1):26–34.

79. Zhang X, Yuan G, Mao L, Niu J, Ding W. Biocorrosion properties of as-extruded Mg–Nd–Zn–Zr alloy compared with commercial AZ31 and WE43 alloys. Mater Lett. 1. Jänner 2012;66(1):209–11.

80. Gu X-N, Zheng Y-F. A review on magnesium alloys as biodegradable materials. Front Mater Sci China. 1. Juni 2010;4(2):111–5.

81. Wirth T, Syed Ali MM, Rauer C, Süß D, Griss P, Syed Ali S. The Blood Supply of the Growth Plate and the Epiphysis: A Comparative Scanning Electron Microscopy and Histological Experimental Study in Growing Sheep. Calcif Tissue Int. April 2002;70(4):312–9.

82. Fan W, Crawford R, Xiao Y. Structural and cellular differences between metaphyseal and diaphyseal periosteum in different aged rats. Bone. 1. Jänner 2008;42(1):81–9.

83. Eliezer A, Witte F. Corrosion Behavior of Magnesium Alloys in Biomedical Environments [Internet]. Bd. 95, Advanced Materials Research. Trans Tech Publications Ltd; 2010 [zitiert 1. März 2021]. S. 17–20. Verfügbar unter: https://www.scientific.net/AMR.95.17

84. Liu C, Xin Y, Tian X, Chu PK. Degradation susceptibility of surgical magnesium alloy in artificial biological fluid containing albumin. J Mater Res. Juli 2007;22(7):1806–14.

85. Wen Z, Wu C, Dai C, Yang F. Corrosion behaviors of Mg and its alloys with different Al contents in a modified simulated body fluid. J Alloys Compd. 20. November 2009;488(1):392–9.

86. Yang L, Zhang E. Biocorrosion behavior of magnesium alloy in different simulated fluids for biomedical application. Mater Sci Eng C. 1. Juni 2009;29(5):1691–6.

87. Ng WF, Chiu KY, Cheng FT. Effect of pH on the in vitro corrosion rate of magnesium degradable implant material. Mater Sci Eng C. 20. Juli 2010;30(6):898–903.

88. Chun-Yan Z, Rong-Chang Z, Cheng-Long L, Jia-Cheng G. Comparison of calcium phosphate coatings on Mg–Al and Mg–Ca alloys and their corrosion behavior in Hank's solution. Surf Coat Technol. 15. August 2010;204(21):3636–40.

89. Kirkland NT, Birbilis N, Staiger MP. Assessing the corrosion of biodegradable magnesium implants: A critical review of current methodologies and their limitations. Acta Biomater. 1. März 2012;8(3):925–36.